

ENERGY LEVEL STRUCTURE AND TRANSITION DATA OF Er²⁺

GEDIMINAS GAIGALAS,¹ PAVEL RYNKUN,¹ LAIMA RADŽIŪTĖ,¹ DAIJI KATO,^{2,3} MASAOMI TANAKA,⁴ AND P. JÖNSSON⁵

¹*Institute of Theoretical Physics and Astronomy, Vilnius University, Saulėtekio Ave. 3, Lithuania*

²*National Institute for Fusion Science, 322-6 Oroshi-cho, Toki 509-5292, Japan*

³*Department of Advanced Energy Engineering, Kyushu University, Kasuga, Fukuoka 816-8580, Japan*

⁴*Astronomical Institute, Tohoku University, Sendai 980-8578, Japan*

⁵*Group for Materials Science and Applied Mathematics, Malmö University, SE-20506, Malmö, Sweden*

(Received February 19, 2020; Revised; Accepted)

Submitted to ApJS

ABSTRACT

The main aim of this paper is to present accurate energy levels of the ground [Xe]4f¹² and first excited [Xe]4f¹¹5d configurations of Er²⁺. The energy level structure of the Er²⁺ ion was computed using the multiconfiguration Dirac-Hartree-Fock and relativistic configuration interaction (RCI) methods, as implemented in the GRASP2018 program package. The Breit interaction, self-energy and vacuum polarization corrections were included in the RCI computations. The zero-first-order approach was used in the computations. Energy levels with the identification in *LS* coupling for all (399) states belonging to the [Xe]4f¹² and [Xe]4f¹¹5d configurations are presented. Electric dipole (E1) transition data between the levels of these two configurations are computed. The accuracy of these data are evaluated by studying the behaviour of the transition rates as functions of the gauge parameter as well as by evaluating the cancellation factors. The core electron correlations were studied using different strategies. Root-mean-square deviations obtained in this study for states of the ground and excited configurations from the available experimental or semi-empirical data are 649 cm⁻¹, and 747 cm⁻¹, respectively.

Keywords: atomic data, radiative transfer, opacity, chemically peculiar stars, neutron stars

Corresponding author: Gediminas Gaigalas
gediminas.gaigalas@tfai.vu.lt

Corresponding author: Pavel Rynkun
pavel.rynkun@tfai.vu.lt

1. INTRODUCTION

Erbium is a lanthanide element with $Z = 68$ and it has 6 stable isotopes. The isotopes are generated by different processes. Isotopes with $A = 162$ are produced by the p process (proton capture), with $A = 167, 170$ by the r process (rapid neutron capture), with $A = 164$ by the p or the s process (slow neutron capture) and with $A = 166, 168$ by the r or the s process (Jaschek & Jaschek 1995). Since Er can be generated by the r process, which can occur in the mergers of neutron star (NS), the atomic spectra of this element is of interest to a wide community of astrophysicists dealing with stellar nuclear synthesis. The contribution of this element to the opacity of NS ejecta should be tested (e.g., Kasen et al. 2017; Tanaka et al. 2018, 2019), but even the energy levels of first excited configuration have not been fully presented.

Ions of erbium have been observed in different types of stars. In the chemically peculiar (CP) stars, high abundances of lanthanide elements compared with solar values are observed. In particular, Er III has been identified in the spectra of CP stars of the upper main sequence (in the silicon star HD 192913 by Cowley & Crosswhite (1978); in the CP A star HR 465 by Cowley & Greenberg (1987)). Cowley & Mathys (1998) have identified lines in the range 5445-6587 Å in spectra of the extreme peculiar star HD 101065 (Przybylski's star). In such stars the strongest spectral lines belong to the lanthanides rather than the iron group elements. In the above spectral range lines of Er III at λ 6393.69, 5881.76 and 5988.39 Å appear.

The critical compilation of the energy levels of this ion, from (Martin & Zalubas 1978), is based on a previous analysis by Spector (1973) of 24 levels for odd and 18 levels for even configurations, respectively. Re-evaluation of the energy levels was done by Wyart et al. (1974a,b); Wyart & Bauche-Arnoult (1981). For these investigations they used a semi-empirical parametric method. More recently, the analysis of the spectrum of Er III was revised by Wyart et al. (1997), and the number of identified energy levels increased from 45 to 115, including some levels of the $4f^{11}7s$ configuration.

Biémont et al. (2001) have measured radiative lifetimes of seven excited states of the $4f^{11}6p$ configuration using time-resolved laser-induced fluorescence following two-photon excitation. Theoretical computation was done in frame of relativistic Hartree-Fock including core-polarization effects.

The aim of this paper is to provide accurate calculations of Er III, which can contribute to the stellar spectroscopy and understanding of opacities in NS mergers. All levels of the ground $[\text{Xe}]4f^{12}$ and first ex-

cited $[\text{Xe}]4f^{11}5d$ configurations of Er^{2+} are analysed in this paper. Different core correlation effects and their inclusion strategies are presented. The energy levels of these configurations and the corresponding electric dipole (E1) transition parameters were computed using the GRASP2018 (Fischer et al. 2019) package. Computations are based on the multiconfiguration Dirac-Hartree-Fock (MCDHF) and relativistic configuration interaction (RCI) methods. The zero-first-order method was tested for various cases.

2. GENERAL THEORY

2.1. Computational procedure

The MCDHF method used in the present paper is based on the Dirac-Coulomb (DC) Hamiltonian

$$H_{DC} = \sum_{i=1}^N (c \boldsymbol{\alpha}_i \cdot \mathbf{p}_i + (\beta_i - 1)c^2 + V_i^N) + \sum_{i>j}^N \frac{1}{r_{ij}} \quad (1)$$

where V^N is the monopole part of the electron-nucleus Coulomb interaction, $\boldsymbol{\alpha}$ and β are the 4×4 Dirac matrices, and c is the speed of light in atomic units. The atomic state functions (ASFs) were obtained as linear combinations of symmetry adapted configuration state functions (CSFs)

$$\Psi(\gamma P J M) = \sum_{j=1}^{N_{CSFs}} c_j \Phi(\gamma_j P J M). \quad (2)$$

Here J and M are the angular quantum numbers and P is parity. γ_j denotes other appropriate labeling of the configuration state function j , for example orbital occupancy and coupling scheme. Normally the label γ of the atomic state function is the same as the label of the dominating CSF, see also section 2.3. For these calculations the spin-angular approach (Gaigalas & Rudzikas 1996; Gaigalas et al. 1997), which is based on the second quantization in coupled tensorial form, on the angular momentum theory in three spaces (orbital, spin, and quasispin) and on the reduced coefficients of fractional parentage, was used. It allows us to study configurations with open f -shells without any restrictions. The CSFs are built from products of one-electron Dirac orbitals. Based on a weighted energy average of several states, the so-called extended optimal level (EOL) scheme (Dyall et al. 1989), both the radial parts of the Dirac orbitals and the expansion coefficients were optimized to self-consistency in the relativistic self-consistent field procedure (Fischer et al. 2016).

2.2. Zero-first-order method

The CSF space can be divided into two parts according to Brillouin-Wigner perturbation theory (Lindgren & Morrison 1982; Kato et al. 2001):

i) a principal part (P), which contains CSFs that account for the major parts of the wave functions and is referred to as a zero-order partitioning;

ii) an orthogonal complementary part (Q), which contains CSFs that represent minor corrections and is referred to as a first-order partitioning.

Interaction between P and Q is assumed to be the lowest-order perturbation. The total energy functional is partitioned into the zero-order part ($H^{(0)}$) and the residual part (V). The Dirac-Fock energy functional is chosen as the zero-order part; the residual part then represents a correlation energy functional. The second-order Brillouin-Wigner perturbation theory then leads to,

$$(E - H_{QQ}^{(0)})^{-1} V_{QP} \Psi_P = \Psi_Q,$$

$$\left[H_{PP}^{(0)} + V_{PP} + V_{PQ} (E - H_{QQ}^{(0)})^{-1} V_{QP} \right] \Psi_P = E \Psi_P \quad (3)$$

The above equations define the first-order correlation operator and the second-order effective Hamiltonian operator for the P -space, respectively. In the brackets of the second equation, the first and second terms compose the total energy functional in the P -space, and the third term represents the second-order correction to the correlation energy functional in the P -space. The non-linear effective Hamiltonian equation is written in a linearized form,

$$\begin{pmatrix} H_{PP}^{(0)} + V_{PP} & V_{PQ} \\ V_{QP} & H_{QQ}^{(0)} \end{pmatrix} \begin{pmatrix} \Psi_P \\ \Psi_Q \end{pmatrix} = E \begin{pmatrix} \Psi_P \\ \Psi_Q \end{pmatrix}. \quad (4)$$

The requirement that the total energy functional (E) is stationary with respect to variations in spin-orbitals ($\{\phi\}$) under the normalization and the orthogonality conditions leads to a set of the Euler-Lagrange equations,

$$\frac{\delta E[\{\phi\}]}{\delta \phi_a} = \mu_a \phi_a + \sum_{b \neq a} \mu_{ab} \phi_b, \quad (5)$$

where $\{\mu\}$ are the Lagrange multipliers. The above equations are nothing but reduced MCDHF equations. That is to say, an apparent connection between the second-order Brillouin-Wigner perturbation energy functional and a set of reduced MCDHF equations is provided.

Block $H_{QQ}^{(0)}$ is diagonal in the Hamiltonian matrix (eq. 4). As a result, computation time and size required for the construction of the Hamiltonian matrix are reduced.

This method, named as zero-first-method (ZF), has the potential for taking a very large configuration space into account, which is almost unachievable by full MCDHF and RCI methods, and for allowing accurate calculation to be performed with relatively small computational resources provided the Q -space contributes perturbatively to the P -space.

2.3. Relativistic configuration interaction method

The RCI method taking into account Breit and quantum electrodynamic (QED) corrections (Grant 2007; Fischer et al. 2016), was used in the computations. The transverse photon interaction (Breit interaction)

$$H_{\text{Breit}} = - \sum_{i < j}^N \left[\alpha_i \cdot \alpha_j \frac{\cos(\omega_{ij} r_{ij}/c)}{r_{ij}} + (\alpha_i \cdot \nabla_i)(\alpha_j \cdot \nabla_j) \frac{\cos(\omega_{ij} r_{ij}/c) - 1}{\omega_{ij}^2 r_{ij}^2 / c^2} \right] \quad (6)$$

was included in the Hamiltonian. The photon frequencies ω_{ij} , used for calculating the matrix elements of the transverse photon interaction, were taken as the difference of the diagonal Lagrange multipliers associated with the Dirac orbitals (McKenzie et al. 1980).

In the present calculations, the ASFs were obtained as expansions over jj -coupled CSFs. To provide the LSJ labeling system, the ASFs were transformed from a jj -coupled CSF basis into an LSJ -coupled CSF basis using the method developed by Gaigalas et al. (2017).

2.4. Computation of transition parameters

The evaluation of radiative electric dipole (E1) transition data (transition probabilities, oscillator strengths) between two states: $\gamma' P' J' M'$ and $\gamma P J M$, built on different and independently optimized orbital sets is non-trivial. The transition data can be expressed in terms of the transition moment, which is defined as

$$\langle \Psi(\gamma P J) \| \mathbf{T}^{(1)} \| \Psi(\gamma' P' J') \rangle = \sum_{j,k} c_j c'_k \langle \Phi(\gamma_j P J) \| \mathbf{T}^{(1)} \| \Phi(\gamma'_k P' J') \rangle, \quad (7)$$

where $\mathbf{T}^{(1)}$ is the transition operator. The calculation of the transition moment breaks down to the task of summing up reduced matrix elements between different CSFs. The reduced matrix elements can be evaluated using standard techniques assuming that both left and right hand CSFs are formed from the same orthonormal set of spin-orbitals. This constraint is severe, since a high-quality and compact wave function requires orbitals optimized for a specific electronic state, for an example, see (Fritzsche & Grant 1994). To get around

the problems of having a single orthonormal set of spin-orbitals, the wave function representations of the two states, i.e. $\gamma'P'J'M'$ and γPJM were transformed in such way that the orbital sets became biorthonormal (Olsen et al. 1995). Standard methods were then used to evaluate the matrix elements of the transformed CSFs.

The reduced matrix elements are expressed via spin-angular coefficients $d_{ab}^{(1)}$ and operator strengths as:

$$\langle \Phi(\gamma_j P J) \| \mathbf{T}^{(1)} \| \Phi(\gamma'_k P' J') \rangle = \sum_{a,b} d_{ab}^{(1)} \langle n_a l_a j_a \| \mathbf{T}^{(1)} \| n_b l_b j_b \rangle. \quad (8)$$

Allowing for the fact that we are now using Brink-and-Satchler type reduced matrix elements, we have

$$\langle n_a l_a j_a \| \mathbf{T}^{(1)} \| n_b l_b j_b \rangle = \left(\frac{(2j_b + 1)\omega}{\pi c} \right)^{1/2} (-1)^{j_a - 1/2} \begin{pmatrix} j_a & 1 & j_b \\ \frac{1}{2} & 0 & -\frac{1}{2} \end{pmatrix} \overline{M}_{ab} \quad (9)$$

where \overline{M}_{ab} , is the radiative transition integral defined by Grant (1974). The latter integral can be written $\overline{M}_{ab} = \overline{M}_{ab}^e + G\overline{M}_{ab}^l$, where G is the gauge parameter. When $G = 0$ we get the Coulomb (velocity) gauge, whereas for $G = \sqrt{2}$ we get the Babushkin (length) gauge. In the general case, the gauge dependence has a parabolic form with respect to the gauge parameter (G axis) (Rudzikas 2007; Gaigalas et al. 2010). This dependence may also be used for the evaluation of the accuracy of the results. The more accurate the wave functions, the closer the parabola is to a straight line.

For electric dipole transitions the Babushkin and Coulomb gauges give the same value of the transition moment for exact solutions of the Dirac-equation (Grant 1974). For approximate solutions the transition moments differ, and the quantity dT , defined as (Ekman et al. 2014)

$$dT = \frac{|A_l - A_v|}{\max(A_l, A_v)}, \quad (10)$$

where A_l and A_v are transition rates in length and velocity form, can be used as a measure of the uncertainty of the computed rate.

In the present work also the cancellation factor (CF), which shows cancellation effects in the computation of transition parameters was investigated. The cancellation factor is defined as (Cowan 1981; Zhang et al. 2013)

$$CF = \left(\frac{\left| \sum_j \sum_k c_j \langle \Phi(\gamma_j P J) \| \mathbf{T}^{(1)} \| \Phi(\gamma'_k P' J') \rangle c'_k \right|}{\sum_k \sum_j |c_j \langle \Phi(\gamma_j P J) \| \mathbf{T}^{(1)} \| \Phi(\gamma'_k P' J') \rangle c'_k|} \right)^2 \quad (11)$$

To calculate CFs some modifications to the GRASP2018 (Fischer et al. 2019) package were done. A small value

of the CF, for example less than 0.1 or 0.05 (values are given in (Cowan 1981)), indicates that the calculated transition parameter, such as transition rate or oscillator strength, is affected by a strong cancellation effect. Transition parameters with small CF are often associated with large uncertainties.

3. COMPUTATIONAL STRATEGIES

The study of the Er^{2+} ion, as well as of the other lanthanides, is quite a complex task because of the open f shells. For systems with open f shells, the number of CSFs increases very rapidly when including various electron correlation effects. Computations for such systems using standard schemes are extremely demanding. For this reason new computational strategies were developed and tested for Er^{2+} .

To obtain good wave functions, various electron correlation effects were investigated. The ZF method was applied to reduce computational resources in different steps of the calculations and to facilitate the inclusion of more electron correlation effects. The final wave functions were used to compute electric dipole (E1) transition data between the levels of the two configurations. The computational strategies will be discussed in more details in the sections below.

3.1. Generation of initial wave functions and active space construction

The first step of the wave function generation was an MCDHF computation of the $[\text{Xe}]4f^{12}$ configuration. In the second step, orbitals from the first step were kept frozen and used for the $[\text{Xe}]4f^{11}5d$ configuration, for which only the $5d$ orbitals ($5d+$ and $5d-$ in relativistic notation) were optimized. In the tables, such an initial computation in two steps will be referred to as a computation for the multireference (MR) space of CSFs. The orbitals belonging to the $[\text{Xe}]4f^{12}$ configuration were kept frozen to get correct order for the states of the ground and excited configurations. A similar technique for the generation of the initial wave functions was already applied for Nd ions (Gaigalas et al. 2019).

In the following steps of the computation, active spaces (AS) of CSFs were generated by allowing single-double (SD) or single-restricted-double (SrD) substitutions from only the valence shells or from valence and core shells of both configurations to the orbital spaces (OS): $OS_1 = \{6s, 6p, 6d, 5f\}$, ..., $OS_4 = \{9s, 9p, 9d, 8f, 7g, 7h\}$. When a new OS is being computed, the previous orbitals are frozen. In Table 1 the number of CSFs used in the computations for the even and odd states is given. The strategies mentioned in this Table will be described below in greater detail.

The Breit interaction and QED effects were included in RCI calculations. These corrections were taken into account in all strategies.

Table 1. Summary of Active Space Constructions for the MCDHF and RCI Computations.

Strategy and AS	No. of CSFs		ZF
	Even	Odd	
SD 4f AS ₁	25 618	407 606	<i>P</i>
AS ₂	115 146	2 414 665	<i>P + Q</i>
AS ₃	326 187	7 986 088	<i>P + Q</i>
AS ₄	649 673	16 859 203	<i>P + Q</i>
SD 5d AS ₁	25 618	538 902	<i>P</i>
AS ₂	115 146	2 868 718	<i>P + Q</i>
AS ₃	326 187	8 958 563	<i>P + Q</i>
AS ₄	649 673	18 527 744	<i>P + Q</i>
SD 5p AS ₂	369 343	11 769 255	
SD 5s AS ₂	193 028	4 745 781	
SrD 5p 5d AS ₂	337 325	10 720 590	
SD 5s 5d AS ₂	193 028	5 584 829	
SrD 5s 5p 5d AS ₂	414 383	13 402 965	
SD 5s 5p 5d AS ₂	476 274	19 482 860	

NOTE—The number of CSFs for the even and odd parities are given for each computational strategy and AS.

3.2. Valence-valence electron correlations

Two strategies for including valence-valence (VV) electron correlations were investigated. In the first, the **SD 4f** strategy, the orbitals of which were used in all other strategies (**SD 5d**, **SD 5p**, **SD 5s**, **SrD 5p 5d**, **SD 5s 5d**, **SrD 5s 5p 5d**, **SD 5s 5p 5d** for these only RCI computations were performed), SD substitutions were allowed only from the *4f* valence shell of both configurations to the different orbital spaces. Later, separate computations were done for AS₂ for the even and odd parities and continued for the AS₃, built from the OS₃ orbital space. In the second strategy, the **SD 5d** strategy, SD substitutions were allowed from both valence (*4f* and *5d*) shells to the different orbital spaces. Results of these investigations are presented in Table 2 and will be discussed in section 4.1.

3.3. Core-valence and core-core electron correlations

The contribution of core-valence (CV) and core-core (CC) electron correlation effects to the energy levels was studied in RCI calculations by allowing SD or SrD substitutions from core (*5p*, *5s*) shells. Results of these computations are presented in Table 3. The orbital spaces are the same as described in section 3.1. The column labeling is similar, for example, the notation **SD 5p** means that SD substitutions were done from the *4f* and *5p* shells. In some computational schemes restrictions for the substitutions were applied. SrD substitutions in the **SrD 5p 5d** strategy mean that SD substitutions were done from the *4f* and *5d* shells, but from the *5p* shell only S substitutions were allowed. In the **SrD 5s 5p 5d** strategy restrictions are applied to the *5s* and *5p* shells by allowing only S substitutions from these shells.

A summary of the active spaces of the different strategies, including core-valence and core-core electron correlation, is displayed in Table 1. From the Table it is seen that substitutions from core shells rapidly increase the number of CSFs. The contribution of these correlations effects to energy levels will be presented in Section 4.2.

3.4. Electron correlations using the zero-first-order method

The ZF method was applied to the **SD 4f** and **SD 5d** strategies and tested at different steps of the computations to reduce the computational load. These results are presented in Tables 4 and 5. Firstly, the ZF method was applied to the MCDHF calculation in the **SD 4f** strategy for AS₂. The results of these calculations, performed separately for the even and odd configurations, are marked as **ZF^{MCDHF}**. For the AS_{2,3,4} active spaces the AS₁ space was used as the principal (*P*) part. The principal part was selected based on the convergence of the energies, see section 4.1. The sizes of the *P* and *P + Q* spaces used in the calculations are given in Table 1. Orbitals from the **SD 4f ZF^{MCDHF}** strategy were used in the RCI calculations for the **SD 4f ZF^{MCDHF}_{RCI}**, **SD 5d ZF^{MCDHF}**, and **SD 5d ZF^{MCDHF}_{RCI}** strategies.

The ZF approach was also used in the RCI calculations. The results are displayed in Tables 4, 5 and referred to as **ZF_{RCI}**. The last columns of the Tables present the results of RCI computations using the ZF method based on orbitals from the **ZF^{MCDHF}** calculations. These results are referred to as **ZF^{MCDHF}_{RCI}**.

4. ENERGY LEVELS RESULTS

Parts of the computed energy spectra from different strategies (described in section 3) are presented in Tables 2 - 6. The labels of the energy levels are given in *LS* notation which are taken from NIST (Kramida et al. 2019), or ordered by energy values for fixed *J* value

(POS). The notation $4f^N (2S+1)L^{Nr} n'l' (2S'+1)L'$ is used for the level labels. Intermediate quantum numbers define parents levels $4f^N (2S+1)L^{Nr}$, where N is electron number in the $4f$ shell, $(2S+1)$ is multiplicity, Nr is a sequential index number representing the group labels νWU for the term, and L is orbital quantum number (see Gaigalas et al. (1998) in more details). Energies in parentheses are from semi-empirical (SE) calculations by Wyart et al. (1997). The total amount of energy levels presented in the NIST (Kramida et al. 2019) database and in the paper (Wyart et al. 1997) for the ground and first excited configuration is only 64. The accuracy of computed energy spectra was evaluated by comparing results with the NIST/(SE) data and calculating the relative difference $\Delta E/E = (E_{NIST/(SE)} - E)/E_{NIST/(SE)}$.

4.1. Convergence and valence-valence electron correlations

Table 2 displays the results when just VV correlations (SD 4f and SD 5d strategies) are included. Using the SD 4f strategy we infer that the wave function relaxation for AS_2 , resulting from separate computations for the even and odd parities, in comparison to the computations where the even and odd parities are computed together, has small effect on the energy levels. It moderately increases the transition energy value by 0.15% (0.09% for levels of ground configuration and 0.15% for levels of excited configuration). For this comparison all 399 levels were included.

The convergence of the obtained energies was evaluated by the following equation $\Delta E/E = (E_{AS_N} - E_{AS_{N-1}})/E_{AS_{N-1}}$. The relative difference ($\overline{\Delta E/E} = \frac{\sum |\Delta E_i/E_i|}{N}$) between active space AS_2 and AS_3 using the SD 4f strategy (when all 399 levels are included) is about 2.6%. By analyzing the results we observe that energies for some J values converge much faster than for others. This is seen from Figure 1, where the convergence for the lowest states of the $4f^{11}5d$ configuration with $J = 0-11$ is presented. For example, the difference between AS_2 and AS_3 for $J = 0$ is about 5% while for lowest state with $J = 6$ it reaches 13%. After the studies of energy levels with different J values, we observed that the lower energy levels converge much slower than the higher energy levels for a fixed J value (see Figure 2). From the Figure we see that even the third level converges much faster than the first one and the agreement between the energies for the last two active spaces is up to 0.3%. In conclusion, the active space has inconsiderable influence on the higher levels as compared to the lowest ones. The upper levels converge much faster.

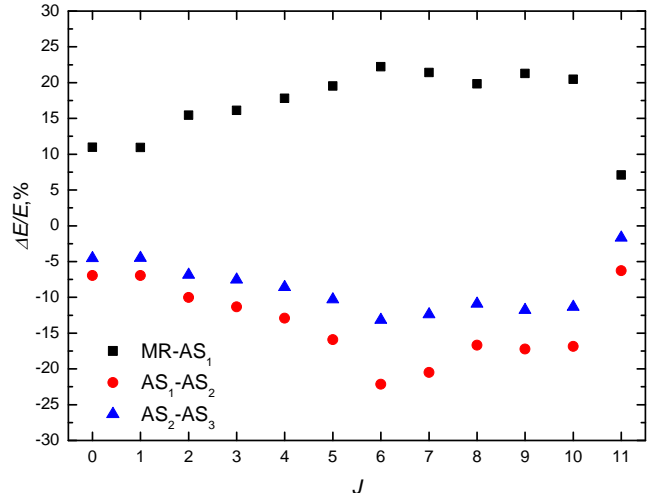


Figure 1. Convergence of the lowest states of the $4f^{11}5d$ configuration with $J = 0 - 11$ in the energy spectrum (SD 4f strategy).

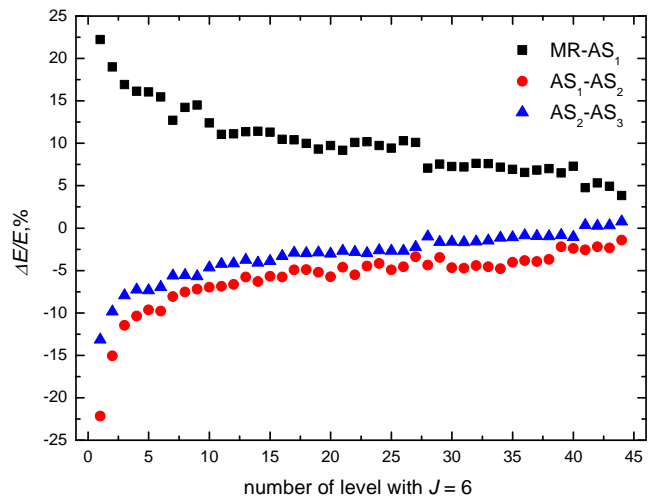


Figure 2. Convergence of all energy values of the $4f^{11}5d$ configuration with $J = 6$ (SD 4f strategy).

The lowest levels according to Hund's first rule have the largest multiplicity. For a given set of eigenstates, the lowest state will have largest multiplicity. Almost all the lowest levels for each J in case of the $4f^{11}5d$ configuration have the largest multiplicity (except $J = 9$), and all these levels converge slower than the higher ones (as it can be seen from Figures 2 and 4). However, even in the set of levels with the largest multiplicity, a large differences in convergence is observable (see Figures 1 and 3). From these Figures it can also be seen that the CSFs from the AS_1 (black squares) have the largest influence. The first active space has a larger influence on energy levels in the SD 5d strategy than in the SD 4f strategy.

Table 2. Energy Levels from RCI Calculations Using the **SD 4f** and **SD 5d** Strategies.

LS	POS	JP	NIST/(SE)	SD 4f								SD 5d	
				MR	Orthogonal		AS ₂	AS ₃	AS ₂	AS ₃			
					AS ₁	AS ₂							
4f ¹² 3H	1	6+	0.00	0	0	0	0	0	0	0	0	0	
4f ¹² 3F	1	4+	5081.79	6335	6142	5898	5895 / -16.00	5744 / -13.03	5895 / -16.00	5744 / -13.03	5895 / -16.00	5744 / -13.03	
4f ¹² 3H	1	5+	6969.78	6673	6733	6786	6784 / 2.66	6805 / 2.36	6784 / 2.66	6805 / 2.36	6784 / 2.66	6805 / 2.36	
4f ¹² 3H	2	4+	10785.48	11089	11036	10957	10958 / -1.60	10889 / -0.96	10958 / -1.60	10889 / -0.96	10958 / -1.60	10889 / -0.96	
4f ¹² 3F	1	3+	(12472.55)	14166	13908	13557	13566 / -8.77	13282 / -6.49	13566 / -8.77	13282 / -6.49	13566 / -8.77	13282 / -6.49	
4f ¹² 3F	1	2+	(13219.80)	15578	15236	14815	14825 / -12.14	14446 / -9.28	14825 / -12.14	14446 / -9.28	14825 / -12.14	14446 / -9.28	
4f ¹² 1G	3	4+	(18383.59)	18387	18391	18377	18360 / 0.13	18381 / 0.01	18360 / 0.13	18381 / 0.01	18360 / 0.13	18381 / 0.01	
4f ¹¹ (4I ¹) 5d 5G	1	6-	16976.09	19978	15540	18872	18983 / -11.82	21480 / -26.53	14673 / 13.56	16073 / 5.32	14673 / 13.56	16073 / 5.32	
4f ¹¹ (4I ¹) 5d 5H	1	7-	17647.76	20984	16495	19770	19877 / -12.63	22337 / -26.57	15613 / 11.53	17006 / 3.64	15613 / 11.53	17006 / 3.64	
4f ¹¹ (4I ¹) 5d 3L	1	9-	18976.74	22664	17843	20827	20916 / -10.22	23382 / -23.21	16725 / 11.87	18204 / 4.07	16725 / 11.87	18204 / 4.07	
4f ¹¹ (4I ¹) 5d 5I	1	8-	19918.17	23811	19088	22181	22273 / -11.82	24699 / -24.00	17988 / 9.69	19380 / 2.70	17988 / 9.69	19380 / 2.70	
4f ¹¹ (4I ¹) 5d 5L	1	10-	20470.13	23320	18548	21587	21673 / -5.88	24130 / -17.88	17644 / 13.81	19158 / 6.41	17644 / 13.81	19158 / 6.41	
4f ¹¹ (4I ¹) 5d 5K	2	9-	21688.17	25556	20625	23583	23664 / -9.11	26085 / -20.27	19561 / 9.81	21006 / 3.15	19561 / 9.81	21006 / 3.15	
4f ¹¹ (4I ¹) 5d 5G	1	5-	22016.77	25908	20848	24065	24164 / -9.75	26648 / -21.04	19890 / 9.66	21285 / 3.32	19890 / 9.66	21285 / 3.32	
4f ¹¹ (4I ¹) 5d 5H	2	6-	22606.07	26785	21696	24867	24963 / -10.43	27418 / -21.29	20716 / 8.36	22102 / 2.23	20716 / 8.36	22102 / 2.23	
4f ¹¹ (4I ¹) 5d 5I	2	8-	22951.42	27237	22101	25006	25085 / -9.30	27514 / -19.88	20903 / 8.93	22321 / 2.75	20903 / 8.93	22321 / 2.75	
4f ¹¹ (4I ¹) 5d 5I	2	7-	23302.78	81645	22982	25958	26039 / -11.74	28459 / -22.13	21733 / 6.73	23103 / 0.86	21733 / 6.73	23103 / 0.86	
4f ¹¹ (4I ¹) 5d 5L	3	8-	25482.12	30201	24501	27376	27453 / -7.73	29916 / -17.40	23276 / 8.66	24757 / 2.85	23276 / 8.66	24757 / 2.85	
4f ¹¹ (4I ¹) 5d 5H	3	5-	26192.66	31455	25931	29019	29109 / -11.13	31551 / -20.46	24808 / 5.29	26162 / 0.12	24808 / 5.29	26162 / 0.12	
4f ¹¹ (4I ¹) 5d 5K	3	7-	26579.91	31832	26197	29141	29220 / -9.93	31644 / -19.05	24959 / 6.10	26367 / 0.80	24959 / 6.10	26367 / 0.80	
	1	4-	(26648.59)	31020	25496	28690	28786 / -8.02	31252 / -17.27	24556 / 7.85	25947 / 2.63	24556 / 7.85	25947 / 2.63	
	2	4-	(29469.40)	34371	28921	32019	32112 / -8.97	34506 / -17.09	27877 / 5.40	29198 / 0.92	27877 / 5.40	29198 / 0.92	
	3	4-	(30750.22)	36329	31536	34481	34590 / -12.49	36669 / -19.25	30274 / 1.55	31299 / -1.78	30274 / 1.55	31299 / -1.78	
	4	4-	(32196.96)	38241	32841	35729	35818 / -11.25	38077 / -18.27	31408 / 2.45	32609 / -1.28	31408 / 2.45	32609 / -1.28	
	5	4-	(33033.10)	39637	33991	36713	36800 / -11.40	38990 / -18.03	32374 / 2.00	33454 / -1.27	32374 / 2.00	33454 / -1.27	
	6	4-	(35903.96)	43048	37724	40326	40430 / -12.61	42276 / -17.75	36133 / -0.64	36946 / -2.90	36133 / -0.64	36946 / -2.90	
	7	4-	(37608.12)	45043	39093	41818	41896 / -11.40	44068 / -17.18	37438 / 0.45	38533 / -2.46	37438 / 0.45	38533 / -2.46	
	8	4-	(39667.36)	46418	41110	43706	43809 / -10.44	45645 / -15.07	39556 / 0.28	40364 / -1.76	39556 / 0.28	40364 / -1.76	
	9	4-	(40580.40)	46896	41790	44350	44448 / -9.53	46293 / -14.08	40165 / 1.02	41000 / -1.03	40165 / 1.02	41000 / -1.03	
	10	4-	(46937.23)	47841	42249	44753	44848 / 4.45	46678 / 0.55	40498 / 13.72	41266 / 12.08	40498 / 13.72	41266 / 12.08	
	3	9-	(27471.61)	31838	25998	28861	28932 / -5.32	31400 / -14.30	24896 / 9.37	26416 / 3.84	24896 / 9.37	26416 / 3.84	
	3	6-	(27472.46)	32771	27231	30271	30355 / -10.49	34985 / -27.35	26082 / 5.06	27443 / 0.11	26082 / 5.06	27443 / 0.11	
	4	6-	(28777.74)	35231	29549	32540	32618 / -13.34	35063 / -21.84	28112 / 2.31	29360 / -2.02	28112 / 2.31	29360 / -2.02	
	5	6-	(30283.09)	35487	29796	32595	32668 / -7.88	36114 / -19.25	28454 / 6.04	29857 / 1.41	28454 / 6.04	29857 / 1.41	
	6	6-	(31095.82)	36376	30755	33686	33767 / -8.59	36114 / -16.14	29549 / 4.98	30894 / 0.65	29549 / 4.98	30894 / 0.65	
	7	6-	(33191.53)	39104	34132	36805	36889 / -11.14	38955 / -17.36	32635 / 1.68	33718 / -1.59	32635 / 1.68	33718 / -1.59	
	8	6-	(33875.19)	41285	35416	38012	38090 / -12.44	40207 / -18.69	33618 / 0.76	34659 / -2.31	33618 / 0.76	34659 / -2.31	
	9	6-	(35856.62)	43309	37029	39631	39697 / -10.71	41952 / -17.00	35430 / 1.19	36666 / -2.26	35430 / 1.19	36666 / -2.26	
	10	6-	(36570.10)	43513	38120	40683	40776 / -11.50	42673 / -16.69	36480 / 0.25	37345 / -2.12	36480 / 0.25	37345 / -2.12	
	3	5-	(27870.83)	34210	28464	31164	31235 / -12.07	33646 / -20.72	26706 / 4.18	27992 / -0.43	26706 / 4.18	27992 / -0.43	
	4	5-	(29995.62)	35316	29934	32954	33042 / -10.16	35388 / -17.98	28760 / 4.12	30057 / -0.20	28760 / 4.12	30057 / -0.20	
	5	5-	(31214.52)	36805	31724	34665	34758 / -11.35	36967 / -18.43	30474 / 2.37	31638 / -1.36	30474 / 2.37	31638 / -1.36	
	6	5-	(32614.37)	38071	33095	35892	35994 / -10.36	38025 / -16.59	31714 / 2.76	32739 / -0.38	31714 / 2.76	32739 / -0.38	
	7	5-	(33704.29)	40276	34638	37366	37449 / -11.11	39616 / -17.54	33073 / 1.87	34182 / -1.42	33073 / 1.87	34182 / -1.42	
	8	5-	(36330.81)	43191	37249	39952	40031 / -10.18	42203 / -16.16	35735 / 1.64	36870 / -1.48	35735 / 1.64	36870 / -1.48	
	9	5-	(36655.60)	44613	38939	41535	41618 / -13.54	43638 / -19.05	37138 / -1.32	38054 / -3.81	37138 / -1.32	38054 / -3.81	
	10	5-	(39265.81)	47531	41949	44443	44536 / -13.42	46335 / -18.00	40220 / -2.43	41002 / -4.42	40220 / -2.43	41002 / -4.42	
	11	5-	(40857.10)	47534	42220	44961	45058 / -10.28	46878 / -14.74	40672 / 0.45	41476 / -1.51	40672 / 0.45	41476 / -1.51	
	12	5-	(46552.18)	48691	42922	45419	45507 / 2.25	47406 / -1.84	41210 / 11.48	42034 / 9.71	41210 / 11.48	42034 / 9.71	
	13	5-	(48747.15)	50473	44655	47228	47313 / 2.94	49233 / -1.00	42975 / 11.84	43871 / 10.00	42975 / 11.84	43871 / 10.00	
	4	8-	(28555.40)	33718	27798	30612	30680 / -7.44	33109 / -15.95	26563 / 6.98	28010 / 1.91	26563 / 6.98	28010 / 1.91	
	5	8-	(31701.46)	36985	30873	33614	33681 / -6.24	36102 / -13.88	29611 / 6.59	31074 / 1.98	29611 / 6.59	31074 / 1.98	
	4	7-	(28818.44)	34225	28372	31253	31327 / -8.70	33744 / -17.09	27034 / 6.19	28431 / 1.34	27034 / 6.19	28431 / 1.34	
	5	7-	(29610.99)	35023	29079	31884	31953 / -7.91	34373 / -16.08	27752 / 6.28	29159 / 1.53	27752 / 6.28	29159 / 1.53	
	6	7-	(32559.55)	38684	32648	35309	35372 / -8.64	37743 / -15.92	31168 / 4.27	32535 / 0.08	31168 / 4.27	32535 / 0.08	
	7	7-	(36636.87)	40135	34251	36905	36973 / -0.92	39291 / -7.25	32864 / 10.30	34212 / 6.62	32864 / 10.30	34212 / 6.62	
	1	3-	(29466.42)	34203	28690	31847	31943 / -8.40	34353 / -16.58	27718 / 5.93	29057 / 1.39	27718 / 5.93	29057 / 1.39	
	2	3-	(31846.16)	37048	31225	34313	34404 / -8.03	36802 / -15.56	30216 / 5.12	31554 / 0.92	30216 / 5.12	31554 / 0.92	
	3	3-	(33185.64)	39693	34892	37685	37798 / -13.90	39691 / -19.61	33433 / -0.75	34279 / -3.29	33433 / -0.75	34279 / -3.29	
	4	3-	(36167.30)	43947	38081	40661	40736 / -12.63	42934 / -18.71	36191 / -0.07	37278 / -3.07	36191 / -0.07	37278 / -3.07	
	5	3-	(37812.87)	44279	39414	41981	42093 / -11.32	43938 / -16.20	37805 / 0.02	38620 / -2.13	37805 / 0.02	38620 / -2.13	
	6	3-	(38924.30)	45611	40313	42866	42968 / -10.39	44779 / -15.04	38621 / 0.78	39395 / -1.21	38621 / 0.78	39395 / -1.21	
	7	3-	(40407.72)	47120	41753	44221	44318 / -9.68	46177 / -14.28	39948 / 1.14	40754 / -0.86	39948 / 1.14	40754 / -0.86	
	1	2-	(38563.97)	43843	31760	41645	34941 / 9.39	37339 / 3.17	30760 / 20.24	32092 / 16.78	30760 / 20.24	32092 / 16.78	

NOTE—The relative difference compared with NIST/(SE) data is given in percent.

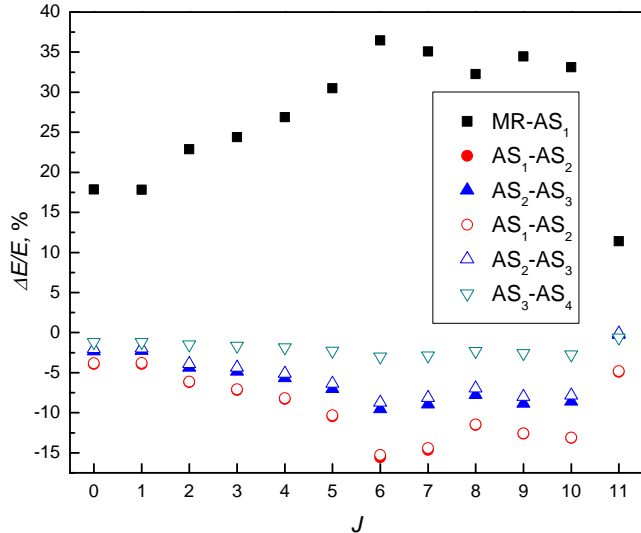


Figure 3. Convergence of the lowest states of $4f^{11}5d$ configuration with $J = 0, 11$ in the energy spectrum. Results are obtained using the **SD 5d** strategy (open symbols mark the results when the **ZF^{MCDHF}** approach at $AS_{2,3,4}$ is applied).

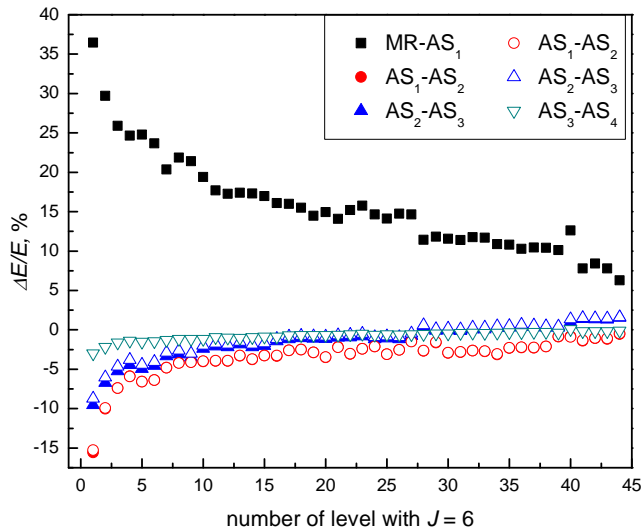


Figure 4. Convergence of all energy values of the $4f^{11}5d$ configuration with $J = 6$. Results are obtained using the **SD 5d** strategy (open symbols mark the results when the **ZF^{MCDHF}** approach at $AS_{2,3,4}$ is applied).

The results of the **SD 4f** strategy substantially disagree with NIST/(SE) data (see Table 2) for states of the $4f^{11}5d$ configuration, and after adding one more layer (AS_3) to the computations, the disagreement increases. From the Table it is seen that after including substitutions from the $5d$ shell (**SD 5d** strategy) the results agree much better. The averaged uncertainty of obtained results from the **SD 5d** strategy at AS_2 is around 5.6% comparing with NIST or SE data. By studying

the convergence of the results obtained using the **SD 5d** strategy we see similar trends as those from the **SD 4f** strategy. Firstly, energies for different J values converge differently. Secondly, lower energy levels converge much slower than the higher energy levels. But in case of the **SD 5d** strategy the energies converge much faster comparing with the **SD 4f** strategy (see Figures 3 and 4). For example, the difference between AS_2 and AS_3 for $J = 0$ is about 2.3% and 9.5% for lowest state with $J = 6$.

4.2. Studies of core-valence and core-core electron correlations

The investigations of core-core and core-valence electron correlations contributions to the transition energies are presented in Table 3. From the Table it is seen that by including substitutions just from the valence shell ($4f$) and core shells ($5p$) or ($5s$) (**SD 5p** or **SD 5s** strategy) the results are in worse agreement with NIST/(SE). In case of the **SD 5p** strategy this disagreement is very large. The relative difference compared with NIST/(SE) data is reduced when substitutions from $4f$, $5d$ and $5p$ or $5s$ shells are allowed. The averaged uncertainty of the obtained results from strategies **SrD 5p 5d**, **SD 5s 5d**, **SrD 5s 5p 5d**, **SD 5s 5p 5d** is similar, around 5-7% comparing with NIST or SE data. As was mentioned above, inclusion of the substitutions from the core shells ($5p$ or $5s$) increases the number of CSFs dramatically (see Table 1). So for further investigations substitutions from the $5p$ and $5s$ shells were neglected.

4.3. Optimal strategy for electron correlations

The **SD 5d** strategy was chosen as the optimal strategy considering achieved accuracy of the results and the computational resources needed for the calculations. The main goal of this work is to obtain accurate energy levels of the ground and first excited configurations of Er^{2+} . So we give priority to balanced electron correlation effects which improves the energy separations.

4.4. Impact of the zero-first-order method

The ZF method was applied at different stages of the calculations to reduce computation resources, as it was described in Section 3.4. The impact of the ZF method was studied using the **SD 4f** and **SD 5d** strategies. In the investigations of the effect of ZF on the energy levels all 399 states were included. The zero-first-order method (see **SD 4f ZF^{MCDHF}** column in Table 4) has up to 0.08% impact on the values of the energy levels at AS_3 if all levels are compared. From Table 5 we see that the ZF method for MCDHF calculations (see **SD 5d ZF^{MCDHF}** column) affects on average the values of

Table 3. Energy Levels from RCI Calculations Including CV and CC Electron Correlations.

<i>LS</i>	POS	JP	NIST/(SE)	SD 5p	SD 5s	SrD 5p 5d	SD 5s 5d	SrD 5s 5p 5d	SD 5s 5p 5d
				<i>AS</i> ₂	<i>AS</i> ₂	<i>AS</i> ₂	<i>AS</i> ₂	<i>AS</i> ₂	<i>AS</i> ₂
$4f^{12} 3H$	1	6+	0.00	0	0	0	0	0	0
$4f^{12} 3F$	1	4+	5081.79	5816 / -14.46	5816 / -14.44	5791 / -13.96	5816 / -14.44	5710 / -12.37	5751 / -13.16
$4f^{12} 3H$	1	5+	6969.78	6773 / 2.83	6777 / 2.77	6784 / 2.67	6777 / 2.77	6778 / 2.75	6755 / 3.08
$4f^{12} 3H$	2	4+	10785.48	10875/ -0.83	10894/ -1.01	10880/ -0.88	10894/ -1.01	10823/ -0.35	10809/ -0.22
$4f^{12} 3F$	1	3+	(12472.55)	13387/ -7.33	13387/ -7.33	13362/ -7.13	13387/ -7.33	13184/ -5.70	13223/ -6.02
$4f^{12} 3F$	1	2+	(13219.80)	14599/ -10.44	14603/ -10.47	14576/ -10.26	14603/ -10.47	14354/ -8.58	14399/ -8.92
$4f^{12} 1G$	3	4+	(18383.59)	18305/ 0.43	18345/ 0.21	18323/ 0.33	18345/ 0.21	18317/ 0.36	18276/ 0.58
$4f^{11} (4I^1) 5d 5G$	1	6-	16976.09	41934/ -147.02	19831/ -16.82	14992/ 11.69	14262/ 15.99	14781/ 12.93	18184/ -7.11
$4f^{11} (4I^1) 5d 5H$	1	7-	17647.76	42676/ -141.82	20691/ -17.24	15783/ 10.57	15143/ 14.19	15518/ 12.07	18929/ -7.26
$4f^{11} (4I^1) 5d 3L$	1	9-	18976.74	44039/ -132.07	21719/ -14.45	17340/ 8.63	16315/ 14.03	17124/ 9.76	20551/ -8.30
$4f^{11} (4I^1) 5d 5I$	1	8-	19918.17	45243/ -127.14	23062/ -15.78	18460/ 7.32	17476/ 12.26	18151/ 8.87	21547/ -8.18
$4f^{11} (4I^1) 5d 5L$	1	10-	20470.13	44910/ -119.39	22487/ -9.85	18326/ 10.47	17280/ 15.59	18186/ 11.16	21705/ -6.03
$4f^{11} (4I^1) 5d 5K$	2	9-	21688.17	46587/ -114.80	24423/ -12.61	19982/ 7.87	19003/ 12.38	19648/ 9.41	23133/ -6.66
$4f^{11} (4I^1) 5d 5G$	1	5-	22016.77	47034/ -113.63	24992/ -13.51	20123/ 8.60	19462/ 11.60	19903/ 9.60	23352/ -6.06
$4f^{11} (4I^1) 5d 5H$	2	6-	22606.07	47717/ -111.08	25765/ -13.97	20849/ 7.77	20236/ 10.49	20578/ 8.97	24017/ -6.24
$4f^{11} (4I^1) 5d 5I$	2	8-	22951.42	48071/ -109.45	25845/ -12.61	21401/ 6.75	20375/ 11.23	21085/ 8.13	24513/ -6.81
$4f^{11} (4I^1) 5d 5I$	2	7-	23302.78	48801/ -109.42	26809/ -15.05	21988/ 5.64	21201/ 9.02	21667/ 7.02	25102/ -7.72
$4f^{11} (4I^1) 5d 5L$	3	8-	25482.12	50537/ -98.32	28240/ -10.82	23883/ 6.28	22844/ 10.35	23653/ 7.18	27097/ -6.34
$4f^{11} (4I^1) 5d 5H$	3	5-	26192.66	51811/ -97.81	29902/ -14.16	24893/ 4.96	24334/ 7.10	24629/ 5.97	28094/ -7.26
$4f^{11} (4I^1) 5d 5K$	3	7-	26579.91	52063/ -95.87	30001/ -12.87	25307/ 4.79	24467/ 7.95	25005/ 5.92	28455/ -7.05
	1	4-	(26648.59)	51645/ -93.80	29603/ -11.09	24778/ 7.02	24111/ 9.52	24539/ 7.92	27997/ -5.06
	2	4-	(29469.40)	54881/ -86.23	32892/ -11.62	28027/ 4.89	27383/ 7.08	27745/ 5.85	31205/ -5.89
	3	4-	(30750.22)	57119/ -85.75	35265/ -14.68	30189/ 1.83	29636/ 3.62	29750/ 3.25	33208/ -7.99
	4	4-	(32196.96)	58399/ -81.38	36546/ -13.51	31442/ 2.34	30866/ 4.14	31119/ 3.35	34581/ -7.40
	5	4-	(33033.10)	59209/ -79.24	37491/ -13.50	32286/ 2.26	31762/ 3.85	31888/ 3.47	35361/ -7.05
	6	4-	(35903.96)	62783/ -74.86	41001/ -14.20	35925/ -0.06	35384/ 1.45	35404/ 1.39	38898/ -8.34
	7	4-	(37608.12)	64261/ -70.87	42577/ -13.21	37261/ 0.92	36805/ 2.14	36852/ 2.01	40347/ -7.28
	8	4-	(39667.36)	66132/ -66.72	44349/ -11.80	39308/ 0.90	38758/ 2.29	38730/ 2.36	42249/ -6.51
	9	4-	(40580.40)	66448/ -63.74	44935/ -10.73	39656/ 2.28	39219/ 3.36	39822/ 4.09	42477/ -4.67
	10	4-	(46937.23)	67135/ -43.03	45403/ 3.27	40249/ 14.25	39676/ 15.47	39660/ 15.50	43170/ 8.03
	3	9-	(27471.61)	52079/ -89.57	29719/ -8.18	25527/ 7.08	24483/ 10.88	25331/ 7.79	28847/ -5.01
	3	6-	(27472.46)	53159/ -93.50	31131/ -13.32	26362/ 4.04	25550/ 7.00	26031/ 5.25	29456/ -7.22
	4	6-	(28777.74)	54968/ -91.01	33363/ -15.93	27916/ 2.99	27508/ 4.41	27532/ 4.33	31022/ -7.80
	5	6-	(30283.09)	55604/ -83.61	33434/ -10.40	28912/ 4.53	27990/ 7.57	28635/ 5.44	32078/ -5.93
	6	6-	(31095.82)	56644/ -82.16	34524/ -11.03	29950/ 3.68	29034/ 6.63	29659/ 4.62	33103/ -6.45
	7	6-	(33191.53)	59528/ -79.35	37535/ -13.08	32780/ 1.24	31945/ 3.75	32302/ 2.68	35782/ -7.80
	8	6-	(33875.19)	60514/ -78.64	38733/ -14.34	33550/ 0.96	32915/ 2.84	33090/ 2.32	36572/ -7.96
	9	6-	(35856.62)	62283/ -73.70	40367/ -12.58	35579/ 0.77	34759/ 3.06	35118/ 2.06	38603/ -7.66
	10	6-	(36570.10)	63109/ -72.57	41345/ -13.06	36358/ 0.58	35683/ 2.43	35777/ 2.17	39291/ -7.44
	3	5-	(27870.83)	53594/ -92.30	32008/ -14.84	26576/ 4.64	26237/ 5.86	26324/ 5.55	29827/ -7.02
	4	5-	(29995.62)	55782/ -85.97	33802/ -12.69	28973/ 3.41	28212/ 5.95	28626/ 4.57	32048/ -6.84
	5	5-	(31214.52)	57489/ -84.17	35477/ -13.66	30691/ 1.68	29870/ 4.31	30284/ 2.98	33712/ -8.00
	6	5-	(32614.37)	58538/ -79.49	36642/ -12.35	31708/ 2.78	31056/ 4.78	31280/ 4.09	34760/ -6.58
	7	5-	(33704.29)	59945/ -77.85	38120/ -13.10	33071/ 1.88	32417/ 3.82	32637/ 3.17	36108/ -7.13
	8	5-	(36330.81)	62518/ -72.08	40690/ -12.00	35739/ 1.63	35088/ 3.42	35311/ 2.81	38797/ -6.79
	9	5-	(36655.60)	63875/ -74.26	42241/ -15.24	36869/ -0.58	36416/ 0.65	36367/ 0.79	39878/ -8.79
	10	5-	(39265.81)	66853/ -70.26	45068/ -14.78	40042/ -1.98	39334/ -0.17	39364/ -0.25	42872/ -9.18
	11	5-	(40857.10)	67312/ -64.75	45623/ -11.66	40402/ 1.11	39864/ 2.43	39789/ 2.61	43274/ -5.92
	12	5-	(46552.18)	67918/ -45.90	46074/ 1.03	41104/ 11.70	40375/ 13.27	40491/ 13.02	44015/ 5.45
	13	5-	(48747.15)	69613/ -42.80	47887/ 1.76	42779/ 12.24	42188/ 13.46	42225/ 13.38	45718/ 6.21
	4	8-	(28555.40)	53567/ -87.59	31423/ -10.04	26983/ 5.51	25993/ 8.97	26630/ 6.74	30107/ -5.43
	5	8-	(31701.46)	56726/ -78.94	34429/ -8.60	30171/ 4.83	29125/ 8.13	29897/ 5.69	33402/ -5.36
	4	7-	(28818.44)	54136/ -87.85	32096/ -11.37	27392/ 4.95	26549/ 7.87	27125/ 5.88	30584/ -6.12
	5	7-	(29610.99)	54836/ -85.19	32698/ -10.43	28183/ 4.82	27212/ 8.10	27868/ 5.89	31307/ -5.73
	6	7-	(32559.55)	58105/ -78.46	36087/ -10.83	31473/ 3.34	30569/ 6.11	31086/ 4.52	34561/ -6.15
	7	7-	(36636.87)	59905/ -63.51	37682/ -2.85	33316/ 9.07	32320/ 11.78	32975/ 9.99	36465/ 0.47
	1	3-	(29466.42)	54751/ -85.81	32737/ -11.10	27882/ 5.38	27240/ 7.56	27608/ 6.31	31075/ -5.46
	2	3-	(31846.16)	57174/ -79.53	35181/ -10.47	30358/ 4.67	29715/ 6.69	30072/ 5.57	33550/ -5.35
	3	3-	(33185.64)	60105/ -81.12	38387/ -15.67	33131/ 0.17	32658/ 1.59	32569/ 1.86	36060/ -8.66
	4	3-	(36167.30)	62975/ -74.12	41433/ -14.56	35937/ 0.64	35629/ 1.49	35597/ 1.58	39120/ -8.16
	5	3-	(37812.87)	64373/ -70.24	42616/ -12.70	37526/ 0.76	36983/ 2.20	36919/ 2.36	40418/ -6.89
	6	3-	(38924.30)	65174/ -67.44	43483/ -11.71	38333/ 1.52	37679/ 3.20	37621/ 3.35	41125/ -5.65
	7	3-	(40407.72)	66462/ -64.48	44850/ -10.99	39574/ 2.06	39111/ 3.21	38966/ 3.57	42478/ -5.12
	1	2-	(38563.97)	57758/ -49.77	35723/ 7.37	30923/ 19.81	30267/ 21.51	30638/ 20.55	34144/ 11.46

NOTE—The relative difference compared with NIST/(SE) data is given in percent.

the energy levels at AS_3 by 0.29%, and in some cases up to 1.01%.

The application of the ZF method for the RCI computation only (see **SD 4f ZF_{RCI}** column in Table 4), has a larger influence on the energy levels; it is up to 2.84% at AS_3 and 1.61% in average for all states. Using the **SD 5d ZF_{RCI}** strategy (see Table 5) the contribution of ZF in RCI is up to 2.69% at AS_3 and 1.45% in average for all states.

When the ZF method was applied for the RCI computations using orbitals from **SD 4f ZF^{MCDHF}** the energies changed in average about 0.5% (**SD 4f ZF^{MCDHF}_{RCI}**) and up to 2.39% for some levels. Using the **SD 5d ZF^{MCDHF}_{RCI}** strategy (see Table 5) the influence of the ZF method is up to 3.95% at AS_3 and 0.66% in average for all states.

From the above study we infer that the impact of the ZF order method on the energy levels is very small in self consistent field computations for both strategies. In the case of the **SD 5d ZF^{MCDHF}** strategy, the effect on the energy levels at AS_3 is only 0.29%.

4.5. Final results

Based on the analysis made in previous sections, the **SD 5d** strategy was chosen as the optimal strategy. Therefore this strategy with the orbitals taken from the **ZF^{MCDHF}** strategy was used to continue computations in AS_4 basis. The final results of the present work are displayed in Table 6 together with NIST and SE data. In first column of the Table we give identifications of energy levels in LS or JJ (see definition in Gaigalas (2020), Eq. (10) and (16)) coupling from our computations, in second column identifications of energy levels are from Wyart et al. (1997). Labels in LS coupling agree with identification given in the NIST database. Labels in JJ coupling are given only for the part of the energy spectra that is used for the comparison with the results of Wyart et al. The averaged uncertainty of the computed energy levels is 5.24%, 2.68%, respectively for states of the ground and excited configurations (see Table 6 **SD 5d ZF^{MCDHF}** strategy AS_4). Root-mean-square (rms) deviations of these results for states of the ground and excited configurations from the NIST/(SE) data are 649 cm^{-1} , and 1571 cm^{-1} , respectively. If the ZF method is used in both the MCDHF and RCI calculations (**SD 5d ZF^{MCDHF}_{RCI}** strategy) the obtained data are in worse agreement (moderately about 7%) with NIST or SE data.

Figure 5 displays the differences between the NIST/(SE) energies and final results of the present study. As it can be seen from Figure 5 and Table 6 (energy levels marked in gray color), there is a significant disagree-

ment between states with the following identifications $J=4$ Pos=10, $J=5$ Pos 12, $J=5$ Pos=13, $J=7$ Pos=7, and $J=2$ Pos=1. Energy differences exceed 2000 cm^{-1} for these five energy levels. It is highly probable that the obtained differences result from incorrect ordering and incomplete identification of energy levels presented by Wyart et al. (1997). Only for one level ($J=7$ Pos=7) from the five above mentioned levels Wyart et al. (1997) give identification in JJ coupling, for the four others only configurations are given. The level is identified as $4F_{9/2} 5d_{5/2}$ ($J=7$). We have transformed ASFs from LS to JJ coupling using the COUPLING program developed by Gaigalas (2020). The level $J=7$ Pos=7 has the $4f^{11}(4I_{9/2}) 5d_{5/2}$ ($9/2, 5/2$) label in JJ coupling which disagree with Wyart et al. By looking at levels which match the identification given by Wyart et al. we see that there is a fit for $J=7$ Pos=8 with identification $4f^{11}(4F_{9/2}) 5d_{5/2}$ ($9/2, 5/2$). If we replace computed energy levels marked in gray color in Table 6 by energy levels suggested in Table 7 (presented by open red circles in Figure 6), agreement with the NIST/(SE) data is much better. The change in the differences between the NIST/(SE) energies and our final results is shown by dashed arrows in Figure 5. The rms deviation for states of the excited configuration (when five of the computed energy levels are replaced) is now only 747 cm^{-1} . By comparing the labels of the levels for which Wyart et al. gives the full identification with our identification in JJ coupling, the labels from both studies agree except for the levels (namely $J=4$ Pos=8, $J=6$ Pos 5, $J=6$ Pos=10, $J=5$ Pos=3, and $J=3$ Pos=1). Level $J=4$ Pos=8 in the present work has the $4f^{11}(4F_{7/2}) 5d_{5/2}$ ($7/2, 5/2$) identification; $J=6$ Pos 5 – $4f^{11}(4I_{9/2}) 5d_{3/2}$ ($9/2, 3/2$); $J=6$ Pos=10 – $4f^{11}(4F_{9/2}) 5d_{5/2}$ ($9/2, 5/2$); $J=5$ Pos=3 – $4f^{11}(4I_{15/2}) 5d_{5/2}$ ($15/2, 5/2$); and $J=3$ Pos=1 – $4f^{11}(4I_{11/2}) 5d_{5/2}$ ($11/2, 5/2$). It was observed that the identification given in (Wyart et al. 1997) for level $J=3$ Pos=1 is incorrect. That level was assigned as $4I_{11/2} 5d_{3/2}$ but such a label for $J=3$ is not consistent with the selection rules. The deeper analysis of uncertainties estimation is complicated because complete identification of energy levels was not given in the paper by Wyart et al. (1997).

The full energy spectrum (energy levels for 399 states) with unique labels and with atomic state function composition in LS coupling using the **SD 5d ZF^{MCDHF}** strategy is presented in machine-readable format in Table 8.

5. TRANSITION DATA RESULTS

The wave functions from the **SD 5d** and **SD 5d ZF^{MCDHF}** strategies, which were chosen as the optimal

Table 4. Energy Levels from RCI Calculations Using the ZF Approach in Different Steps of the Calculations (SD 4f Strategy).

<i>LS</i>	POS	JP	NIST/(SE)	SD 4f		SD 4f ZF ^{MCDHF}		SD 4f ZF ^{RCI}		SD 4f ZF ^{MCDHF} ^{RCI}		
				AS ₂	AS ₃	AS ₂	AS ₃	AS ₂	AS ₃	AS ₂	AS ₃	AS ₄
4f ¹² 3H	1	6+	0.00	0	0	0	0.00	0	0	0	0	0
4f ¹² 3F	1	4+	5081.79	5894	5744	5895	5744	5834	5628	5832	5617	5572
4f ¹² 3H	1	5+	6969.78	6784	6805	6786	6806	6790	6791	6794	6796	6798
4f ¹² 3H	2	4+	10785.48	10957	10889	10961	10889	10912	10786	10915	10785	10766
4f ¹² 3F	1	3+	(12472.55)	13565	13282	13570	13279	13472	13076	13475	13066	13019
4f ¹² 3F	1	2+	(13219.80)	14824	14446	14829	14442	14777	14290	14780	14280	14216
4f ¹² 1G	3	4+	(18383.59)	18359	18381	18361	18388	18188	18116	18187	18108	18053
4f ¹¹ (4I ¹) 5d 5G	1	6-	16976.09	18983	21480	18976	21466	19666	20919	19634	22004	23585
4f ¹¹ (4I ¹) 5d 5H	1	7-	17647.76	19877	22337	19875	22323	20543	21751	20513	22839	24421
4f ¹¹ (4I ¹) 5d 3L	1	9-	18976.74	20916	23382	20933	23369	21593	22753	21577	23859	25438
4f ¹¹ (4I ¹) 5d 5I	1	8-	19918.17	22273	24699	22285	24685	22923	24060	21577	25163	26746
4f ¹¹ (4I ¹) 5d 5L	1	10-	20470.13	21673	24130	21692	24116	22306	23463	22293	24575	26146
4f ¹¹ (4I ¹) 5d 5K	2	9-	21688.17	23664	26085	23687	26071	24285	25387	24275	26504	28084
4f ¹¹ (4I ¹) 5d 5G	1	5-	22016.77	24164	26648	24167	26634	24936	26172	24906	27264	28844
4f ¹¹ (4I ¹) 5d 5H	2	6-	22606.07	24963	27418	24970	27404	25701	26896	25675	27993	29572
4f ¹¹ (4I ¹) 5d 5I	2	8-	22951.42	25085	27514	25111	27501	25736	26835	25726	27954	29535
4f ¹¹ (4I ¹) 5d 5I	2	7-	23302.78	26039	28459	26061	28445	26723	27834	26710	28948	30529
4f ¹¹ (4I ¹) 5d 5L	3	8-	25482.12	27453	29916	27481	29903	28211	29364	28198	30479	32061
4f ¹¹ (4I ¹) 5d 5H	3	5-	26192.66	29109	31551	29122	31537	29877	31044	29853	32145	33715
4f ¹¹ (4I ¹) 5d 5K	3	7-	26579.91	29220	31644	29245	31630	29967	31094	29952	32206	33781
	1	4-	(26648.59)	28786	31252	28792	31238	29595	30816	29565	31908	33482
	2	4-	(29469.40)	32112	34506	32121	34492	32857	33980	32830	35074	36623
	3	4-	(30750.22)	34590	36669	34584	36655	35182	35938	35153	37015	38514
	4	4-	(32196.96)	35818	38077	35831	38064	36504	37462	36482	38560	40091
	5	4-	(33033.10)	36800	38990	36816	38976	37462	38323	37445	39432	40969
	6	4-	(35903.96)	40430	42276	40430	42262	41007	41478	40981	42564	44050
	7	4-	(37608.12)	41896	44068	41919	44054	42533	43359	42519	44467	45981
	8	4-	(39667.36)	43809	45645	43809	45631	44370	44833	44343	45916	47388
	9	4-	(40580.40)	44448	46293	44452	46279	44964	45424	44942	46513	48012
	10	4-	(46937.23)	44848	46678	44856	46664	45435	45881	45412	46975	48464
	3	9-	(27471.61)	28932	31400	28964	31386	29672	30820	29663	31942	33516
	3	6-	(27472.46)	30355	34985	30374	32747	31102	32230	31083	33335	34907
	4	6-	(28777.74)	32618	35063	32642	34972	33310	34342	33300	35463	37023
	5	6-	(30283.09)	32668	36114	32697	35049	33393	34505	33378	35614	37176
	6	6-	(31095.82)	33767	36114	33789	36100	34471	35516	34455	36623	38172
	7	6-	(33191.53)	36889	38955	36909	38941	37476	38145	37462	39243	40744
	8	6-	(33875.19)	38090	40207	38115	40194	38707	39459	38698	40581	42120
	9	6-	(35856.62)	39697	41952	39734	41939	40377	41260	40371	42385	43931
	10	6-	(36570.10)	40776	42673	40787	42659	41303	41822	41287	42926	44426
	3	5-	(27870.83)	31235	33646	31267	33632	31956	33014	31948	34138	35701
	4	5-	(29995.62)	33042	35388	33056	35374	33750	34811	33728	35909	37455
	5	5-	(31214.52)	34758	36967	34768	36954	35395	36273	35374	37363	38877
	6	5-	(32614.37)	35994	38025	35995	38011	36569	37289	36545	38380	39889
	7	5-	(33704.29)	37449	39616	37468	39602	38095	38931	38079	40039	41571
	8	5-	(36330.81)	40031	42203	40054	42189	40688	41505	40673	42564	44138
	9	5-	(36655.60)	41618	43638	41638	43624	42201	42850	42189	43961	45469
	10	5-	(39265.81)	44536	46335	44546	46321	45111	45507	45091	46601	48083
	11	5-	(40857.10)	45058	46878	45063	46864	45575	46024	45554	47116	48588
	12	5-	(46552.18)	45507	47406	45521	47393	46086	46602	46068	47703	49195
	13	5-	(48747.15)	47313	49233	47330	49219	47881	48424	47865	49525	51002
	4	8-	(28555.40)	30680	33109	30715	33095	31424	32525	31416	33650	35232
	5	8-	(31701.46)	33681	36102	33717	36089	34407	35485	34399	36609	38170
	4	7-	(28818.44)	31327	33744	31356	33731	32067	33172	32055	34289	35862
	5	7-	(29610.99)	31953	34373	31987	34359	32699	33791	32689	34913	36491
	6	7-	(32559.55)	35372	37743	35412	37729	36082	37093	36078	38221	39782
	7	7-	(36636.87)	36973	39291	37007	39277	37649	38597	37642	39716	41249
	1	3-	(29466.42)	31943	34353	31949	34339	32712	33871	32682	34961	36516
	2	3-	(31846.16)	34404	36802	34415	36788	35149	36282	35123	37379	38932
	3	3-	(33185.64)	37798	39691	37788	39677	38350	38906	38320	39982	41475
	4	3-	(36167.30)	40736	42934	40763	42920	41406	42218	41394	43330	44849
	5	3-	(37812.87)	42093	43938	42085	43923	42655	43141	42622	44215	45696
	6	3-	(38924.30)	42968	44779	42969	44765	43507	43943	43484	45031	46529
	7	3-	(40407.72)	44318	46177	44324	46163	44847	45302	44827	46395	47874
	1	2-	(38563.97)	34941	37339	34952	37325	35680	36810	35654	37907	39458

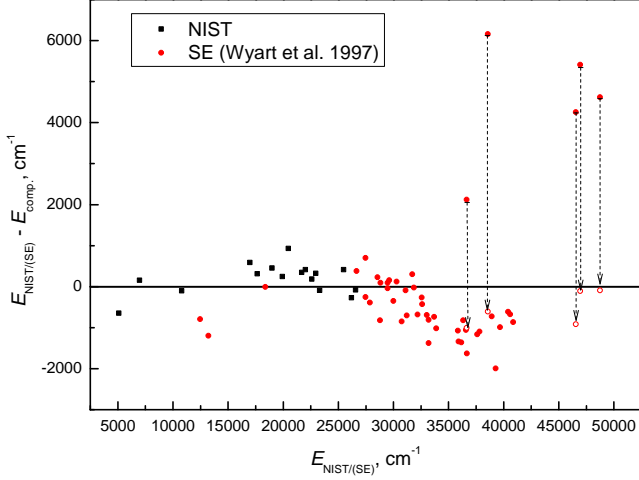


Figure 5. A comparison of energy levels between the NIST or SE values Wyart et al. (1997) and results of the present study. The dashed arrows indicate the improved agreement resulting from a re-identification of the levels in Wyart et al. (1997), see text for details.

computational schemes, were used to compute E1 transition data between states of the $[\text{Xe}]4f^{12}$ and $[\text{Xe}]4f^{11}5d$ configurations. The accuracy of the transition data obtained in this work was evaluated by:

1. calculating parameter dT , which shows the disagreement between the length and velocity forms of the computed transition rates;
2. analyzing the convergence of the computed transition rates in the length and velocity forms;
3. analyzing the dependence of the transition rate on the gauge parameter G ;
4. analyzing the dependence of cancellation factor on the gauge parameter G ;
5. comparing computed transition data with other experimental or theoretical calculations.

For these investigations a few strong transitions have been chosen as examples. The evaluation of transition data will be presented in the sections below.

Computed transition data, such as wavelengths, weighted oscillator strengths, transition rates of E1 along with the accuracy indicator dT , are given in machine-readable format in Table 9.

5.1. Disagreement between the length and velocity and their convergence

In a variational approach the wave functions are optimized on an energy expression. In general this gives a better representation of the outer part of the wave

functions, thus favoring the length form. The velocity form contains a dependence on the transition energy in the matrix element, which may affect the accuracy of the evaluation. Due to the above mentioned reasons, a much slower convergence of the velocity gauge is expected (Ynnerman & Fischer 1995). However, a recent paper by Papoulia et al. (2019), analyzing in detail the convergence properties of transitions in light elements, suggests that transition probabilities in the Coulomb gauge may give the more accurate values. Thus, it is important to systematically study the transition data to see which gauge results in the most rapid convergence.

The convergence of the transition rates in both gauges with the increasing active spaces is presented in Figures 6 and 7. From these Figures it is seen that transition probabilities in the Babushkin gauge are more stable to electron correlation effects than the probabilities in the Coulomb gauge. The dT for the analyzed transitions based on the final AS_4 in the **SD 5d ZF^{MCDHF}** strategy are 12% for $4f^{12} \ ^3P_0 - 4f^{11} \ (^2F^1) \ 5d \ ^3P_1$, 23% for $4f^{12} \ ^1S_0 - 4f^{11} \ (^2F^1) \ 5d \ ^1P_1$ (Figure 6); 3% for $4f^{12} \ ^3P_2 - 4f^{11} \ (^2F^2) \ 5d \ ^1P_1$ and 5% for $4f^{12} \ ^3P_2 - 4f^{11} \ (^2F^1) \ 5d \ ^3P_1$ (Figure 7).

Analyzing the impact of the ZF method on the transition rates, we see that ZF^{MCDHF} AS_3 reduces transition rates compared to those from the **SD 5d** strategy. The transition rates in Coulomb gauge change even more than those in the Babushkin gauge. Transition rates in Babushkin gauge decreases just by a few percent for the analyzed transitions. The above analysis shows that the Babushkin gauge is the preferred one.

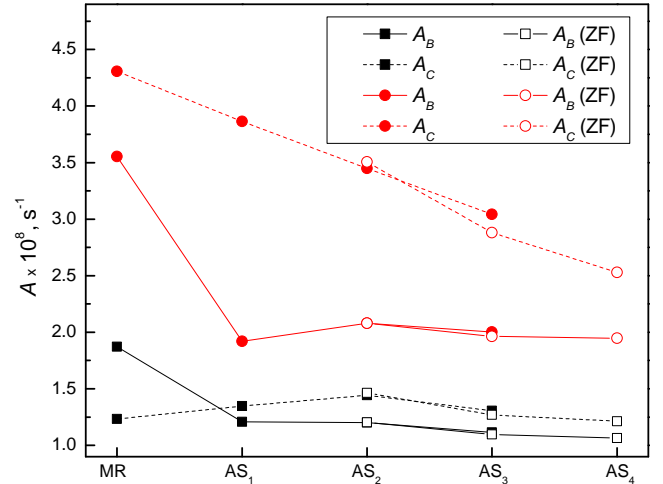


Figure 6. Convergence of E1 transition probabilities using the **SD 5d** strategy (open symbols mark the results when the ZF^{MCDHF} approach is applied). The $4f^{12} \ ^3P_0 - 4f^{11} \ (^2F^1) \ 5d \ ^3P_1$ transition is marked in black and the $4f^{12} \ ^1S_0 - 4f^{11} \ (^2F^1) \ 5d \ ^1P_1$ transition in red.

Table 5. Energy Levels from RCI Calculations Using the ZF Approach in Different Steps of the Calculations (SD 5d Strategy).

<i>LS</i>	POS	JP	NIST/(SE)	SD 5d		SD 5d ZF ^{MCDHF}		SD 5d ZF ^{RCI}		SD 5d ZF ^{MCDHF} _{RCI}	
				AS ₂	AS ₃	AS ₂	AS ₃	AS ₂	AS ₃	AS ₂	AS ₃
4f ¹² 3H	1	6+	0.00	0	0	0	0	0	0	0	0
4f ¹² 3F	1	4+	5081.79	5895	5744	5895	5744	5833	5628	5832	5617
4f ¹² 3H	1	5+	6969.78	6784	6805	6786	6806	6790	6791	6794	6796
4f ¹² 3H	2	4+	10785.48	10958	10889	10961	10890	10912	10786	10916	10786
4f ¹² 3F	1	3+	(12472.55)	13566	13282	13570	13279	13471	13075	13475	13066
4f ¹² 3F	1	2+	(13219.80)	14825	14446	14829	14442	14776	14290	14781	14280
4f ¹² 1G	3	4+	(18383.59)	18360	18381	18361	18388	18187	15728	18188	18109
4f ¹¹ (4I ¹) 5d 5G	1	6-	16976.09	14673	16073	14638	15912	15109	15728	15045	16734
4f ¹¹ (4I ¹) 5d 5H	1	7-	17647.76	15613	17006	15583	16849	16057	16642	15997	17652
4f ¹¹ (4I ¹) 5d 3L	1	9-	18976.74	16725	18204	16721	18057	17194	17734	17150	18766
4f ¹¹ (4I ¹) 5d 5I	1	8-	19918.17	17988	19380	17977	19226	18417	18924	18369	19951
4f ¹¹ (4I ¹) 5d 5L	1	10-	20470.13	17644	19158	17640	19019	18088	18656	18048	19695
4f ¹¹ (4I ¹) 5d 5K	2	9-	21688.17	19561	21006	19562	20861	19985	20485	19947	21528
4f ¹¹ (4I ¹) 5d 5G	1	5-	22016.77	19890	21285	19866	21125	20456	21058	20396	22074
4f ¹¹ (4I ¹) 5d 5H	2	6-	22606.07	20716	22102	20696	21944	21256	21822	21199	22842
4f ¹¹ (4I ¹) 5d 5I	2	8-	22951.42	20903	22321	20906	22170	21357	21837	21318	22881
4f ¹¹ (4I ¹) 5d 5I	2	7-	23302.78	21733	23103	21733	22946	22215	22689	22172	23727
4f ¹¹ (4I ¹) 5d 5L	3	8-	25482.12	23276	24757	23283	24610	23839	24376	23797	25416
4f ¹¹ (4I ¹) 5d 5H	3	5-	26192.66	24808	26162	24796	26001	25368	25881	25315	26907
4f ¹¹ (4I ¹) 5d 5K	3	7-	26579.91	24959	26367	24963	26215	25510	26005	25467	27043
	1	4-	(26648.59)	24556	25947	24533	25789	25166	25762	25104	26776
	2	4-	(29469.40)	27877	29198	27858	29040	28423	28910	28365	29926
	3	4-	(30750.22)	30274	31299	30242	31141	30648	30782	30588	31783
	4	4-	(32196.96)	31408	32609	31401	32446	31894	32225	31845	33250
	5	4-	(33033.10)	32374	33454	32361	33291	32814	33018	32764	34044
	6	4-	(35903.96)	36133	36946	36106	36791	36501	36350	36444	37359
	7	4-	(37608.12)	37438	38533	37440	38367	37872	38055	37829	39088
	8	4-	(39667.36)	39556	40364	39530	40209	39911	39765	39854	40770
	9	4-	(40580.40)	40165	41000	40145	40846	40463	40318	40412	41330
	10	4-	(46937.23)	40498	41266	40482	41108	40866	40650	40815	41666
	3	9-	(27471.61)	24896	26416	24906	26274	25453	26006	25416	27055
	3	6-	(27472.46)	26082	27443	26077	27287	26623	27115	26575	28144
	4	6-	(28777.74)	28112	29360	28123	29190	28598	28957	28561	30003
	5	6-	(30283.09)	28454	29857	28453	29708	29009	29507	28963	30539
	6	6-	(31095.82)	29549	30894	29548	30745	30058	30480	30013	31510
	7	6-	(33191.53)	32635	33718	32634	33567	33025	33092	32982	34114
	8	6-	(33875.19)	33618	34659	33620	34495	34014	34125	33976	35170
	9	6-	(35856.62)	35430	36666	35446	36512	35906	36165	35871	37218
	10	6-	(36570.10)	36480	37345	36467	37193	36781	36644	36736	37669
	3	5-	(27870.83)	26706	27992	26714	27823	27225	27635	27185	28678
	4	5-	(29995.62)	28760	30057	28749	29902	29261	29690	29210	30711
	5	5-	(31214.52)	30474	31638	30459	31484	30890	31115	30839	32127
	6	5-	(32614.37)	31714	32739	31692	32585	32095	32222	32041	33237
	7	5-	(33704.29)	33073	34182	33069	34022	33511	33715	33466	34747
	8	5-	(36330.81)	35735	36870	35735	36714	36193	36386	36149	37420
	9	5-	(36655.60)	37138	38054	37135	37888	37503	37468	37461	38502
	10	5-	(39265.81)	40220	41002	40208	40847	40562	40325	40514	41344
	11	5-	(40857.10)	40672	41476	40651	41317	40976	40841	40924	41852
	12	5-	(46552.18)	41210	42034	41200	41878	41583	41409	41536	42432
	13	5-	(48747.15)	42975	43871	42968	43715	43336	43270	43291	44295
	4	8-	(28555.40)	26563	28010	26576	27863	27113	27607	27076	28658
	5	8-	(31701.46)	29611	31074	29626	30931	30149	30624	30114	31675
	4	7-	(28818.44)	27034	28431	27041	28278	27583	28061	27542	29102
	5	7-	(29610.99)	27752	29159	27763	29008	28303	28778	28264	29825
	6	7-	(32559.55)	31168	32535	31186	32385	31672	32063	31639	33116
	7	7-	(36636.87)	32864	34212	32877	34067	33355	33689	33320	34734
	1	3-	(29466.42)	27718	29057	27694	28899	28290	28822	28228	29834
	2	3-	(31846.16)	30216	31554	30200	31397	30772	31282	30715	32303
	3	3-	(33185.64)	33433	34279	33397	34120	33758	33701	33697	34700
	4	3-	(36167.30)	36191	37278	36197	37110	36645	36799	36603	37835
	5	3-	(37812.87)	37805	38620	37771	38464	38168	38032	38105	39027
	6	3-	(38924.30)	38621	39395	38597	39238	38938	38743	38883	39753
	7	3-	(40407.72)	39948	40754	39930	40596	40253	40068	40203	41083
	1	2-	(38563.97)	30760	32092	30742	31935	31306	31815	31248	32835

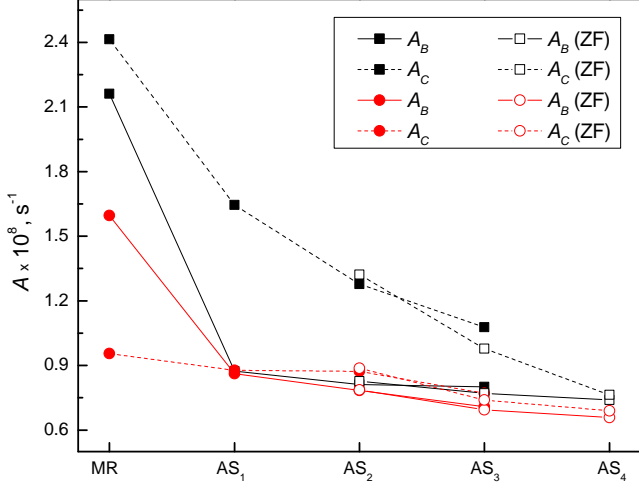


Figure 7. Convergence of E1 transition probabilities using the **SD 5d** strategy (open symbols mark the results when the \mathbf{ZF}^{MCDHF} approach is applied). The $4f^{12} \ ^3P_2 - 4f^{11} \ (^2F^2) \ 5d \ ^1P_1$ transition is marked in black and the $4f^{12} \ ^3P_2 - 4f^{11} \ (^2F^1) \ 5d \ ^3P_1$ transition in red.

5.2. Gauge dependence

In Figures 8–11 the dependence of the transition probabilities for the different active space calculations on the gauge parameter G is displayed. In each of these Figures the position of Coulomb and Babushkin gauges are marked by dotted lines. For some of analyzed transitions the curves of gauge dependence intersect at some point. The cross points are marked by dotted lines and the values are placed on the axis. The curves cross at around $G = 1.7$ (very close to the Babushkin form) for the $4f^{12} \ ^1S_0 - 4f^{11} \ (^2F^1) \ 5d \ ^1P_1$ (Figure 8) and $4f^{12} \ ^3P_2 - 4f^{11} \ (^2F^1) \ 5d \ ^1P_1$ (Figure 10) transitions. For the $4f^{12} \ ^3P_0 - 4f^{11} \ (^2F^1) \ 5d \ ^3P_1$ transition (Figure 9) the most of curves (except the curve of gauge dependence with AS_1) intersect at around $G = 3.4$. In case of the $4f^{12} \ ^3P_2 - 4f^{11} \ (^2F^1) \ 5d \ ^3P_1$ transition (Figure 11) the curves do not intersect at one point. From these Figures we can see that by increasing the active space, the curves of gauge dependence approach straight lines. At AS_4 (final results) these curves are very close to straight lines. It means that the wave functions should be quite accurate.

5.3. Cancellation factor

Figures 12 and 13 show the CF as a function of the increasing active space for the **SD 5d** strategy. From the Figures it is seen that CF in the Babushkin gauge for the analyzed transitions in all active spaces are larger than in the Coulomb gauge. In Figure 14 and 15 we present the dependence of CF on the gauge parameter G using the **SD 5d ZF^{MCDHF}** strategy (at AS_4). The CF is

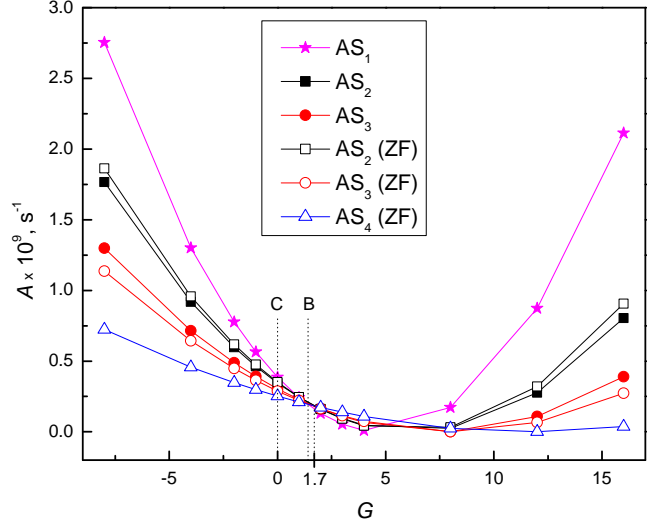


Figure 8. The gauge dependence of the $4f^{12} \ ^1S_0 - 4f^{11} \ (^2F^1) \ 5d \ ^1P_1$ E1 transition probability for the different active space calculations using the **SD 5d** strategy (open symbols mark the results when the \mathbf{ZF}^{MCDHF} approach is applied).

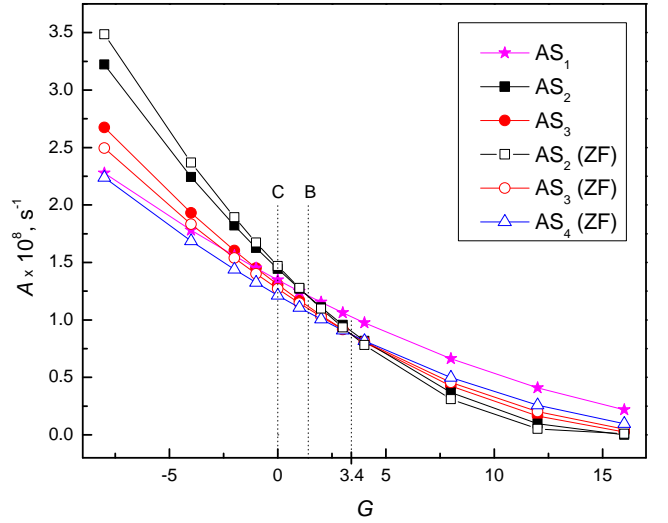


Figure 9. The gauge dependence of the $4f^{12} \ ^3P_0 - 4f^{11} \ (^2F^1) \ 5d \ ^3P_1$ E1 transition probability for the different active space calculations using the **SD 5d** strategy (open symbols mark the results when the \mathbf{ZF}^{MCDHF} approach is applied).

presented for the four analyzed transitions. The CFs in Babushkin gauge for these transitions are much larger than 0.1 or 0.05, and in all cases they are the largest ones. They are even larger than at the cross points, where gauge dependence curves from different active spaces intersect. The CFs in Coulomb gauge for the transitions $4f^{12} \ ^3P_2 - 4f^{11} \ (^2F^2) \ 5d \ ^1P_1$ and $4f^{12} \ ^3P_2 - 4f^{11} \ (^2F^1) \ 5d \ ^3P_1$ (Figure 15) are smaller than 0.05,

Table 6. Comparison of Energy Levels from the Present Calculations Based on the **SD 5d** Strategy and Using the ZF Approach with NIST/SE data.

<i>LS/JJ</i>	label in Wyart et al. (1997)	POS	JP	NIST/(SE)	SD 5d ZF ^{MCDHF}		SD 5d ZF ^{MCDHF} _{RCI}	
					AS ₄		AS ₄	
4f ¹² 3H		1	6+	0.00	0		0	
4f ¹² 3F		1	4+	5081.79	5731/	-12.77	5572 /	-9.65
4f ¹² 3H		1	5+	6969.78	6814/	2.24	6798 /	2.47
4f ¹² 3H		2	4+	10785.48	10890/	-0.97	10766 /	0.18
4f ¹² 3F		1	3+	(12472.55)	13267/	-6.37	13019/	-4.38
4f ¹² 3F		1	2+	(13219.80)	14418/	-9.06	14216/	-7.54
4f ¹² 1G		3	4+	(18383.59)	18393/	-0.05	18053/	1.80
4f ¹¹ (4I ¹) 5d 5G		1	6-	16976.09	16391/	3.44	18186/	-7.13
4f ¹¹ (4I ¹) 5d 5H		1	7-	17647.76	17333/	1.78	19110/	-8.29
4f ¹¹ (4I ¹) 5d 3L		1	9-	18976.74	18524/	2.39	20211/	-6.51
4f ¹¹ (4I ¹) 5d 5I		1	8-	19918.17	19672/	1.24	21401/	-7.44
4f ¹¹ (4I ¹) 5d 5L		1	10-	20470.13	19537/	4.56	21155/	-3.34
4f ¹¹ (4I ¹) 5d 5K		2	9-	21688.17	21342/	1.60	22986/	-5.98
4f ¹¹ (4I ¹) 5d 5G		1	5-	22016.77	21604/	1.87	23527/	-6.86
4f ¹¹ (4I ¹) 5d 5H		2	6-	22606.07	22421/	0.82	24297/	-7.48
4f ¹¹ (4I ¹) 5d 5I		2	8-	22951.42	22629/	1.41	24329/	-6.00
4f ¹¹ (4I ¹) 5d 5I		2	7-	23302.78	23392/	-0.38	25176/	-8.04
4f ¹¹ (4I ¹) 5d 5L		3	8-	25482.12	25069/	1.62	26865/	-5.43
4f ¹¹ (4I ¹) 5d 5H		3	5-	26192.66	26464/	-1.03	28349/	-8.23
4f ¹¹ (4I ¹) 5d 5K		3	7-	26579.91	26661/	-0.31	28490/	-7.19
4f ¹¹ (4I _{11/2}) 5d _{3/2} (11/2, 3/2)	4I _{11/2} 5d _{3/2}	1	4-	(26648.59)	26268/	1.43	28225/	-5.92
4f ¹¹ (4I _{11/2}) 5d _{5/2} (11/2, 5/2)	4f ¹¹ 5d	2	4-	(29469.40)	29509/	-0.13	31348/	-6.37
4f ¹¹ (4F _{9/2}) 5d _{3/2} (9/2, 3/2)	4F _{9/2} 5d _{3/2}	3	4-	(30750.22)	31599/	-2.76	33161/	-7.84
4f ¹¹ (4I _{9/2}) 5d _{3/2} (9/2, 3/2)	4f ¹¹ 5d	4	4-	(32196.96)	32877/	-2.11	34655/	-7.63
4f ¹¹ (4F _{9/2}) 5d _{3/2} (9/2, 3/2)	4f ¹¹ 5d	5	4-	(33033.10)	33728/	-2.10	35450/	-7.32
4f ¹¹ (4F _{7/2}) 5d _{3/2} (7/2, 3/2)	4F _{9/2} 5d	6	4-	(35903.96)	37243/	-3.73	38722/	-7.85
4f ¹¹ (4I _{9/2}) 5d _{5/2} (9/2, 5/2)	4I _{9/2} 5d _{5/2}	7	4-	(37608.12)	38774/	-3.10	40476/	-7.62
4f ¹¹ (4F _{7/2}) 5d _{5/2} (7/2, 5/2)	4F _{7/2} 5d _{3/2}	8	4-	(39667.36)	40658/	-2.50	42126/	-6.20
4f ¹¹ (4S _{3/2}) 5d _{5/2} (3/2, 5/2)	4f ¹¹ 5d	9	4-	(40580.40)	41258/	-1.67	42710/	-5.25
4f ¹¹ (4F _{7/2}) 5d _{3/2} (7/2, 3/2)	4f ¹¹ 5d	10	4-	(46937.23)	41524/	11.53	43024/	8.34
4f ¹¹ (4I _{13/2}) 5d _{5/2} (13/2, 5/2)	4I _{13/2} 5d _{5/2}	3	9-	(27471.61)	26769/	2.56	28508/	-3.77
4f ¹¹ (4I _{13/2}) 5d _{3/2} (13/2, 3/2)	4I _{13/2} 5d _{3/2}	3	6-	(27472.46)	27729/	-0.93	29584/	-7.69
4f ¹¹ (4I _{13/2}) 5d _{5/2} (13/2, 5/2)	4I _{13/2} 5d _{5/2}	4	6-	(28777.74)	29598/	-2.85	31434/	-9.23
4f ¹¹ (4I _{9/2}) 5d _{3/2} (9/2, 3/2)	4I _{11/2} 5d _{3/2}	5	6-	(30283.09)	30162/	0.40	31975/	-5.59
4f ¹¹ (4I _{9/2}) 5d _{3/2} (9/2, 3/2)	4I _{9/2} 5d _{3/2}	6	6-	(31095.82)	31189/	-0.30	32928/	-5.89
4f ¹¹ (4I _{11/2}) 5d _{5/2} (11/2, 5/2)	4f ¹¹ 5d	7	6-	(33191.53)	34004/	-2.45	35490/	-6.93
4f ¹¹ (4I _{11/2}) 5d _{5/2} (11/2, 5/2)	4I _{11/2} 5d _{5/2}	8	6-	(33875.19)	34893/	-3.01	36573/	-7.96
4f ¹¹ (4I _{9/2}) 5d _{5/2} (9/2, 5/2)	4f ¹¹ 5d	9	6-	(35856.62)	36933/	-3.00	38635/	-7.75
4f ¹¹ (4F _{9/2}) 5d _{5/2} (9/2, 5/2)	4I _{9/2} 5d _{5/2}	10	6-	(36570.10)	37627/	-2.89	39036/	-6.74
4f ¹¹ (4I _{15/2}) 5d _{5/2} (15/2, 5/2)	4I _{13/2} 5d _{5/2}	3	5-	(27870.83)	28262/	-1.40	30113/	-8.04
4f ¹¹ (4I _{11/2}) 5d _{3/2} (11/2, 3/2)	4I _{11/2} 5d _{3/2}	4	5-	(29995.62)	30345/	-1.16	32127/	-7.10
4f ¹¹ (4I _{9/2}) 5d _{3/2} (9/2, 3/2)	4f ¹¹ 5d	5	5-	(31214.52)	31916/	-2.25	33507/	-7.34
4f ¹¹ (4F _{9/2}) 5d _{3/2} (9/2, 3/2)	4f ¹¹ 5d	6	5-	(32614.37)	33040/	-1.31	34629/	-6.18
4f ¹¹ (4F _{9/2}) 5d _{3/2} (9/2, 3/2)	4f ¹¹ 5d	7	5-	(33704.29)	34444/	-2.20	36152/	-7.26
4f ¹¹ (4I _{9/2}) 5d _{5/2} (9/2, 5/2)	4f ¹¹ 5d	8	5-	(36330.81)	37154/	-2.27	38817/	-6.84
4f ¹¹ (4F _{9/2}) 5d _{5/2} (9/2, 5/2)	4f ¹¹ 5d	9	5-	(36655.60)	38287/	-4.45	39879/	-8.79
4f ¹¹ (4F _{7/2}) 5d _{3/2} (7/2, 3/2)	4f ¹¹ 5d	10	5-	(39265.81)	41260/	-5.08	42696/	-8.74
4f ¹¹ (2H ² _{11/2}) 5d _{3/2} (11/2, 3/2)	4f ¹¹ 5d	11	5-	(40857.10)	41726/	-2.13	43204/	-5.75
4f ¹¹ (4F _{7/2}) 5d _{5/2} (7/2, 5/2)	4f ¹¹ 5d	12	5-	(46552.18)	42297/	9.14	43795/	5.92
4f ¹¹ (2H ² _{11/2}) 5d _{5/2} (11/2, 5/2)	4f ¹¹ 5d	13	5-	(48747.15)	44128/	9.48	45642/	6.37
4f ¹¹ (4I _{13/2}) 5d _{5/2} (13/2, 5/2)	4I _{13/2} 5d _{5/2}	4	8-	(28555.40)	28325/	0.81	30112/	-5.45
4f ¹¹ (4I _{11/2}) 5d _{5/2} (11/2, 5/2)	4I _{11/2} 5d _{5/2}	5	8-	(31701.46)	31400/	0.95	33108/	-4.44
4f ¹¹ (4I _{11/2}) 5d _{3/2} (11/2, 3/2)	4I _{11/2} 5d _{3/2}	4	7-	(28818.44)	28722/	0.33	30546/	-5.99
4f ¹¹ (4I _{13/2}) 5d _{5/2} (13/2, 5/2)	4I _{13/2} 5d _{5/2}	5	7-	(29610.99)	29454/	0.53	31269/	-5.60
4f ¹¹ (4I _{11/2}) 5d _{5/2} (11/2, 5/2)	4I _{11/2} 5d _{5/2}	6	7-	(32559.55)	32825/	-0.82	34542/	-6.09
4f ¹¹ (4I _{9/2}) 5d _{5/2} (9/2, 5/2)	4F _{9/2} 5d _{5/2}	7	7-	(36636.87)	34516/	5.79	36135/	1.37
4f ¹¹ (4I _{11/2}) 5d _{5/2} (11/2, 5/2)	4I _{11/2} 5d _{3/2}	1	3-	(29466.42)	29374/	0.31	31265/	-6.10
4f ¹¹ (4I _{9/2}) 5d _{5/2} (9/2, 5/2)	4I _{9/2} 5d _{5/2}	2	3-	(31846.16)	31869/	-0.07	33733/	-5.92
4f ¹¹ (4F _{9/2}) 5d _{3/2} (9/2, 3/2)	4F _{9/2} 5d _{3/2}	3	3-	(33185.64)	34565/	-4.16	36072/	-8.70
4f ¹¹ (4I _{9/2}) 5d _{3/2} (9/2, 3/2)	4f ¹¹ 5d	4	3-	(36167.30)	37527/	-3.76	39226/	-8.46
4f ¹¹ (4F _{7/2}) 5d _{3/2} (7/2, 3/2)	4f ¹¹ 5d	5	3-	(37812.87)	38909/	-2.90	40386/	-6.81
4f ¹¹ (4F _{7/2}) 5d _{3/2} (7/2, 3/2)	4f ¹¹ 5d	6	3-	(38924.30)	39652/	-1.87	41122/	-5.65
4f ¹¹ (4F _{9/2}) 5d _{5/2} (9/2, 5/2)	4f ¹¹ 5d	7	3-	(40407.72)	41020/	-1.51	41122/	-5.01
4f ¹¹ (4I _{9/2}) 5d _{5/2} (9/2, 5/2)	4f ¹¹ 5d	1	2-	(38563.97)	32408/	15.96	34263/	11.15

Table 7. The Proposed Energy Levels in Comparison with NIST/(SE) Data and Their Relative Difference (Given in Percent).

JP	NIST/(SE)	iden. in Wyart et al. (1997)	POS	SD 5d ZF ^{MCDHF} (AS ₄)	iden. in present work
4-	(46937.23)		10 → 15	41524/11.53 → 47046/−0.23	
5-	(46552.18)		12 → 16	42297/ 9.14 → 47467/−1.96	
5-	(48747.15)		13 → 17	44128/ 9.48 → 48836/−0.18	
7-	(36636.87)	⁴ F _{9/2} 5d _{5/2}	7 → 8	34516/ 5.79 → 37645/−2.75	4f ¹¹ (⁴ F _{9/2}) 5d _{5/2} (9/2, 5/2)
2-	(38563.97)		1 → 3	32408/15.96 → 39173/−1.58	

Table 8. Energy Levels (in cm^{−1}) and Atomic State Function Composition of the Ground [Xe]4f¹² and First Excited [Xe]4f¹¹5d Configurations for the Er²⁺ ion.

No.	POS	J	P	E	label	comp.
1	1	6	+	0.00	4f ¹² ³ H	0.95
2	1	4	+	5730.98	4f ¹² ³ F	0.56 + 0.29 4f ¹² ¹ G + 0.11 4f ¹² ³ H
3	1	5	+	6813.74	4f ¹² ³ H	0.95
4	2	4	+	10889.64	4f ¹² ³ H	0.59 + 0.29 4f ¹² ³ F + 0.07 4f ¹² ¹ G
5	1	3	+	13267.28	4f ¹² ³ F	0.95
6	1	2	+	14417.89	4f ¹² ³ F	0.81 + 0.13 4f ¹² ¹ D
7	1	6	−	16391.49	4f ¹¹ (⁴ I ¹) 5d ⁵ G	0.75 + 0.13 4f ¹¹ (⁴ I ¹) 5d ⁵ H + 0.02 4f ¹¹ (² K ¹) 5d ³ H
8	1	7	−	17333.10	4f ¹¹ (⁴ I ¹) 5d ⁵ H	0.76 + 0.11 4f ¹¹ (⁴ I ¹) 5d ⁵ I + 0.02 4f ¹¹ (⁴ G ¹) 5d ⁵ H
9	3	4	+	18392.93	4f ¹² ¹ G	0.59 + 0.25 4f ¹² ³ H + 0.11 4f ¹² ³ F
10	1	9	−	18523.58	4f ¹¹ (⁴ I ¹) 5d ³ L	0.43 + 0.33 4f ¹¹ (⁴ I ¹) 5d ⁵ L + 0.17 4f ¹¹ (⁴ I ¹) 5d ⁵ K
11	1	10	−	19537.18	4f ¹¹ (⁴ I ¹) 5d ⁵ L	0.92 + 0.02 4f ¹¹ (² K ¹) 5d ³ M
12	1	8	−	19671.88	4f ¹¹ (⁴ I ¹) 5d ⁵ I	0.44 + 0.28 4f ¹¹ (⁴ I ¹) 5d ⁵ K + 0.15 4f ¹¹ (⁴ I ¹) 5d ³ K
13	2	9	−	21341.61	4f ¹¹ (⁴ I ¹) 5d ⁵ K	0.71 + 0.21 4f ¹¹ (⁴ I ¹) 5d ³ L
14	1	5	−	21604.17	4f ¹¹ (⁴ I ¹) 5d ⁵ G	0.65 + 0.17 4f ¹¹ (⁴ I ¹) 5d ⁵ H + 0.05 4f ¹¹ (⁴ I ¹) 5d ³ G
15	2	6	−	22420.54	4f ¹¹ (⁴ I ¹) 5d ⁵ H	0.54 + 0.16 4f ¹¹ (⁴ I ¹) 5d ⁵ G + 0.11 4f ¹¹ (⁴ I ¹) 5d ⁵ I
16	2	8	−	22628.77	4f ¹¹ (⁴ I ¹) 5d ³ K	0.29 + 0.40 4f ¹¹ (⁴ I ¹) 5d ⁵ I + 0.09 4f ¹¹ (⁴ I ¹) 5d ⁵ L
17	2	7	−	23392.31	4f ¹¹ (⁴ I ¹) 5d ³ I	0.23 + 0.31 4f ¹¹ (⁴ I ¹) 5d ⁵ I + 0.17 4f ¹¹ (⁴ I ¹) 5d ⁵ K
18	3	8	−	25069.42	4f ¹¹ (⁴ I ¹) 5d ⁵ L	0.49 + 0.25 4f ¹¹ (⁴ I ¹) 5d ³ K + 0.20 4f ¹¹ (⁴ I ¹) 5d ³ L
19	1	4	−	26268.28	4f ¹¹ (⁴ I ¹) 5d ⁵ G	0.59 + 0.25 4f ¹¹ (⁴ I ¹) 5d ⁵ H + 0.03 4f ¹¹ (² H ²) 5d ³ F
20	2	5	−	26463.59	4f ¹¹ (⁴ I ¹) 5d ⁵ H	0.45 + 0.24 4f ¹¹ (⁴ I ¹) 5d ³ G + 0.09 4f ¹¹ (⁴ I ¹) 5d ⁵ I

NOTE— Table 8 is published in its entirety in the machine-readable format. Part of the values are shown here for guidance regarding its form and content.

which means that in velocity form there is a strong cancellation effect. For the 4f¹² ³P₀ − 4f¹¹ (²F¹) 5d ³P₁ and 4f¹² ¹S₀ − 4f¹¹ (²F¹) 5d ¹P₁ (Figure 14) transitions, the CF in the Coulomb gauge is around 0.05. The analysis shows that transition data in the Babushkin

gauge are less affected by cancellation effects than transition data in the velocity gauge.

5.4. Comparison with other computations

No experimental transition rates for the studied configurations of Er²⁺ are available. The transition data obtained using the SD 5d ZF^{MCDHF} strategy (at

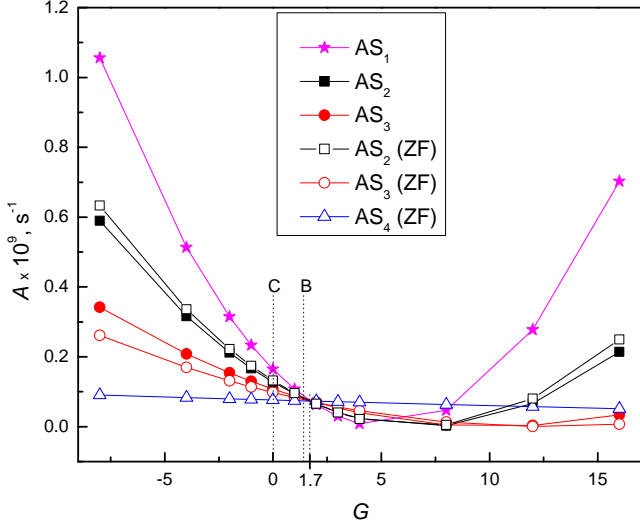


Figure 10. The gauge dependence of the $4f^{12} 3P_2 - 4f^{11} ({}^2F^2) 5d^1 P_1$ E1 transition probability for the different active space calculations using the **SD 5d** strategy (open symbols mark the results when the **ZF^{MCDHF}** approach is applied).

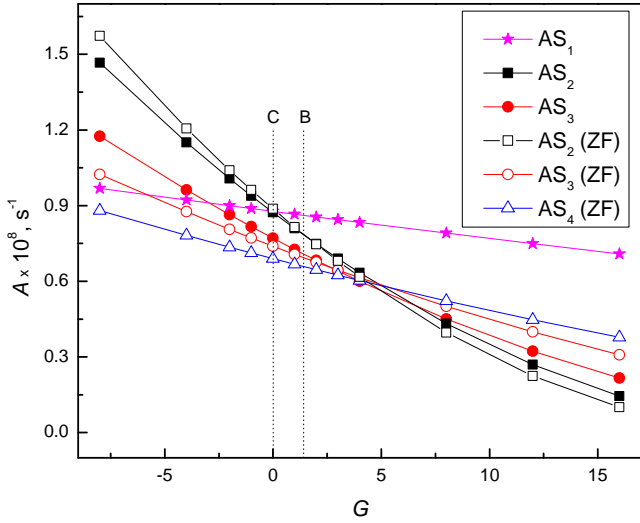


Figure 11. The gauge dependence of the $4f^{12} 3P_2 - 4f^{11} ({}^2F^1) 5d^3 P_1$ E1 transition probability for the different active space calculations using the **SD 5d** strategy (open symbols mark the results when the **ZF^{MCDHF}** approach is applied).

AS_4) are compared with rates presented by Wyart et al. (1997) and Biémont et al. (2001). They used experimental transition wavelengths to compute transition data. Biémont et al. (2001) used the Cowan code and included core-polarization effects in the computations.

Figure 16 presents a comparison of obtained transition wavelengths with experimental data, which were presented in the paper by Wyart et al. (1997). The

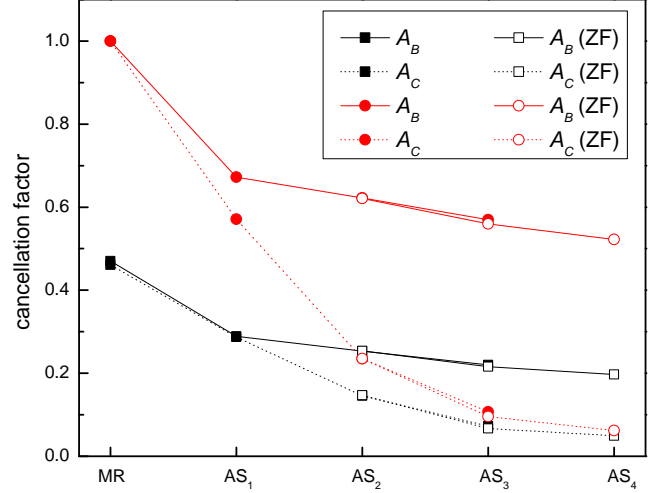


Figure 12. Cancellation factor dependence on the active space. The $4f^{12} 3P_0 - 4f^{11} ({}^2F^1) 5d^3 P_1$ transition is marked in black and the $4f^{12} 1S_0 - 4f^{11} ({}^2F^1) 5d^1 P_1$ transition in red.

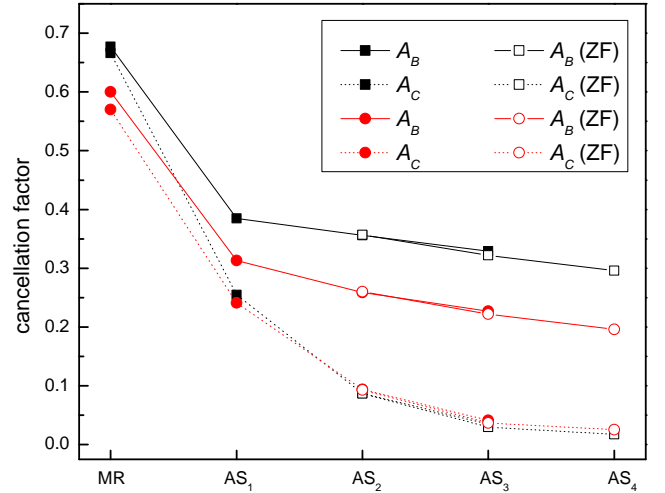


Figure 13. Cancellation factor dependence on the active space. The $4f^{12} 3P_2 - 4f^{11} ({}^2F^2) 5d^1 P_1$ transition is marked in black and the $4f^{12} 3P_2 - 4f^{11} ({}^2F^1) 5d^3 P_1$ transition in red.

agreement between the computed wavelengths and the experimental ones is very good. Almost all compared lines achieve 5% uncertainty. In Figure 17 the comparison of transition rates (given in Babushkin gauge) of the present work with rates available from other computations (Wyart et al. 1997; Biémont et al. 2001) is displayed. It is seen that there is a good agreement with values from other authors for the stronger transitions. However, the transitions presented in the Figure are not the strongest obtained in this work. The strongest transition have rates of the order 10^8 s^{-1} . By applying replacement in the energy levels discussed in Section 4.5

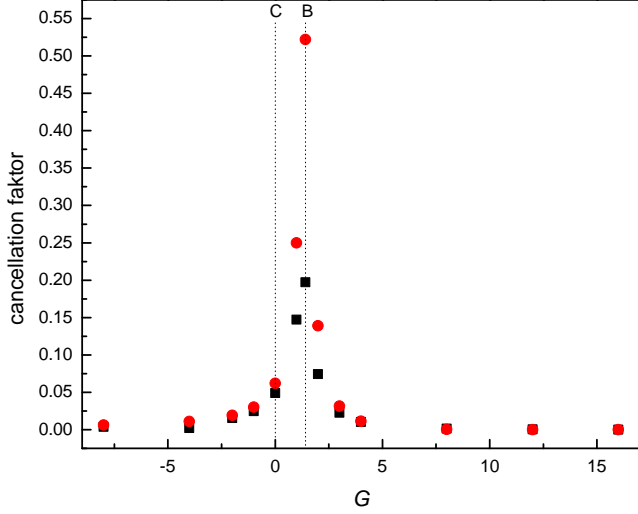


Figure 14. Cancellation factor dependence on gauge using the **SD 5d ZF^{MCDHF}** strategy (at AS_4). The $4f^{12} 3P_0 - 4f^{11} (2F^1) 5d 3P_1$ transition is marked and in black and the $4f^{12} 1S_0 - 4f^{11} (2F^1) 5d 1P_1$ transition is marked in red.

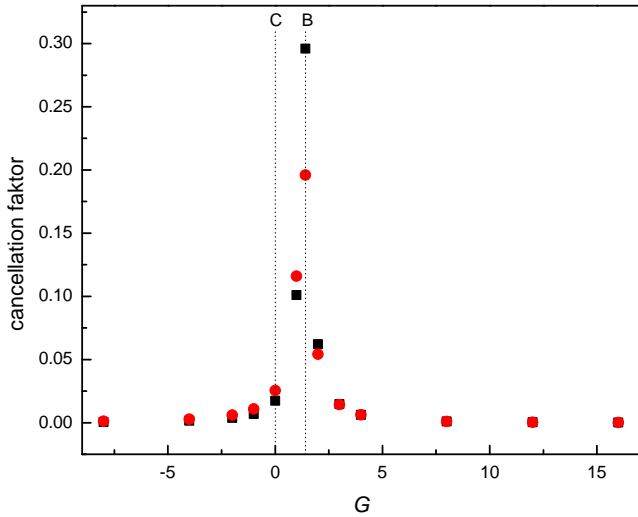


Figure 15. Cancellation factor dependence on gauge using the **SD 5d ZF^{MCDHF}** strategy (at AS_4). The $4f^{12} 3P_2 - 4f^{11} (2F^2) 5d 1P_1$ transition is marked and in black and the $4f^{12} 3P_2 - 4f^{11} (2F^1) 5d 3P_1$ transition is marked in red.

we achieve better agreement for wavelength and transition rate of marked transition (see open symbols in Figures 16 and 17).

6. SUMMARY AND CONCLUSION

In the present paper energy levels of the ground $[Xe]4f^{12}$ and first excited $[Xe]4f^{11}5d$ configurations for Er^{2+} ion were computed using the GRASP2018 package. Transition data for E1 transitions between computed states are presented. The accuracy of the obtained results is evaluated.

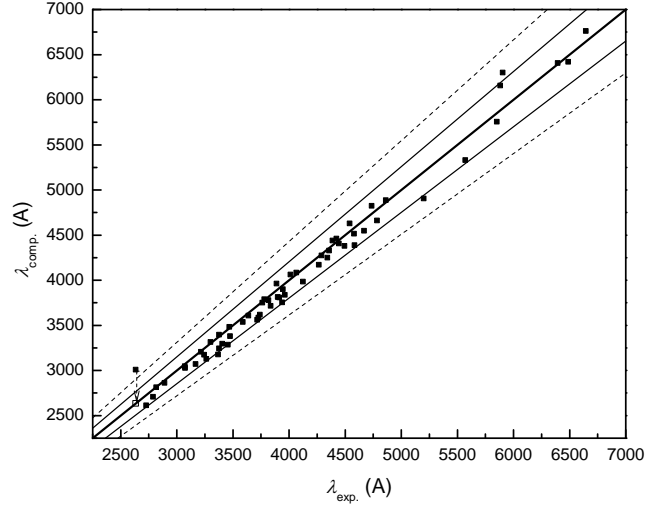


Figure 16. Comparison of transition wavelengths between our computed data (comp.) using the **SD 5d ZF^{MCDHF}** strategy (at AS_4) and experimental data presented in the paper by Wyart et al. Wyart et al. (1997). The thick line corresponds to perfect agreement, while thin solid and dashed lines correspond to 5% and 10% deviations. The dashed arrows indicate the improved agreement by applying replacement in the energy levels discussed in Section 4.5.

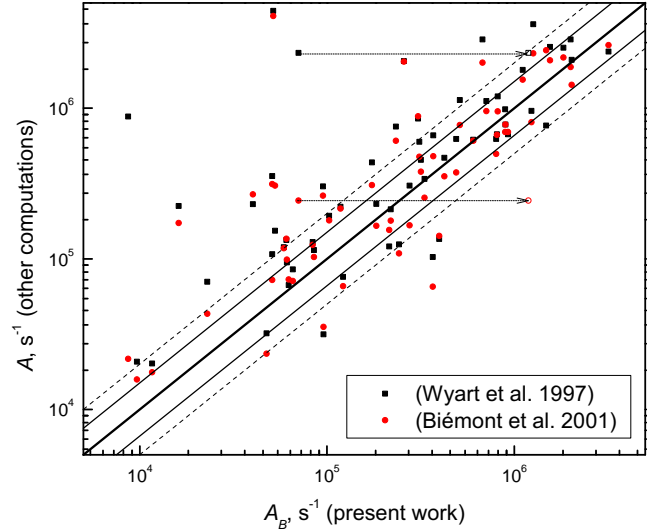


Figure 17. Comparison of transition rates of present work (A is given in Babushkin gauge) with rates presented in Wyart et al. (1997) and Biémont et al. (2001). The data from Wyart et al. (1997) and Biémont et al. (2001) are marked by black squares and the red circles correspond to the results by Biémont et al. Biémont et al. (2001). The thick line corresponds to perfect agreement, while the thin solid and dashed lines correspond to deviations by factors of 1.5 and 2.0, respectively. The dashed arrows indicate the improved agreement by applying replacement in the energy levels discussed in Section 4.5.

Table 9. Transition Energies ΔE (in cm⁻¹), Transition Wavelengths λ (in Å), Weighted Oscillator Strengths gf and Transition Rates A (in s⁻¹) for E1 Transitions of the Er²⁺ Ion.

No.(u)	J_u	P_u	state(u)	No.(l)	J_l	P_l	state(l)	ΔE	λ	A	gf	dT
7	6	-	$4f^{11} (4I^1) 5d^5 G$	1	6	+	$4f^{12} 3H$	16391	6100.73	8.417E+02	6.106E-05	0.855
7	6	-	$4f^{11} (4I^1) 5d^5 G$	3	5	+	$4f^{12} 3H$	9577	10440.87	1.402E+01	2.978E-06	0.919
8	7	-	$4f^{11} (4I^1) 5d^5 H$	1	6	+	$4f^{12} 3H$	17333	5769.31	4.336E-01	3.246E-08	1.000
14	5	-	$4f^{11} (4I^1) 5d^5 G$	1	6	+	$4f^{12} 3H$	21604	4628.74	5.100E+04	1.802E-03	0.711
14	5	-	$4f^{11} (4I^1) 5d^5 G$	2	4	+	$4f^{12} 3F$	15873	6299.93	6.063E+04	3.968E-03	0.685
14	5	-	$4f^{11} (4I^1) 5d^5 G$	3	5	+	$4f^{12} 3H$	14790	6761.13	9.658E+03	7.280E-04	0.771
14	5	-	$4f^{11} (4I^1) 5d^5 G$	4	4	+	$4f^{12} 3H$	10714	9333.12	4.760E+03	6.837E-04	0.780
14	5	-	$4f^{11} (4I^1) 5d^5 G$	9	4	+	$4f^{12} 1G$	3211	31140.62	4.578E+01	7.321E-05	0.962
15	6	-	$4f^{11} (4I^1) 5d^5 H$	1	6	+	$4f^{12} 3H$	22420	4460.20	3.113E+05	1.207E-02	0.551
15	6	-	$4f^{11} (4I^1) 5d^5 H$	3	5	+	$4f^{12} 3H$	15606	6407.46	1.165E+04	9.318E-04	0.700
17	7	-	$4f^{11} (4I^1) 5d^5 I$	1	6	+	$4f^{12} 3H$	23392	4274.91	7.104E+05	2.920E-02	0.517
19	4	-	$4f^{11} (4I^1) 5d^5 G$	2	4	+	$4f^{12} 3F$	20537	4869.19	8.829E+02	2.824E-05	0.084
19	4	-	$4f^{11} (4I^1) 5d^5 G$	3	5	+	$4f^{12} 3H$	19454	5140.19	9.666E+03	3.446E-04	0.595
19	4	-	$4f^{11} (4I^1) 5d^5 G$	4	4	+	$4f^{12} 3H$	15378	6502.53	2.340E+03	1.335E-04	0.796
19	4	-	$4f^{11} (4I^1) 5d^5 G$	5	3	+	$4f^{12} 3F$	13001	7691.72	1.108E+04	8.847E-04	0.728
19	4	-	$4f^{11} (4I^1) 5d^5 G$	9	4	+	$4f^{12} 1G$	7875	12697.85	9.995E+01	2.174E-05	0.682
20	5	-	$4f^{11} (4I^1) 5d^5 H$	1	6	+	$4f^{12} 3H$	26463	3778.78	2.335E+05	5.499E-03	0.746
20	5	-	$4f^{11} (4I^1) 5d^5 H$	2	4	+	$4f^{12} 3F$	20732	4823.32	3.069E+05	1.177E-02	0.615
20	5	-	$4f^{11} (4I^1) 5d^5 H$	3	5	+	$4f^{12} 3H$	19649	5089.10	3.843E+01	1.641E-06	0.983
20	5	-	$4f^{11} (4I^1) 5d^5 H$	4	4	+	$4f^{12} 3H$	15573	6420.98	6.119E+04	4.160E-03	0.701

NOTE—All transition data are in length form. dT is the relative difference of the transition rates in length and velocity form as given by equation 10. Table 9 is published in its entirety in the machine-readable format. Part of the values are shown here for guidance regarding its form and content.

From the studies of the Er²⁺ ion, and also from the previous investigations of Nd ions, it was observed that in such calculations to get the correct order of ground and excited configurations it is important to freeze the wave functions of ground configuration.

The valence-valence, core-valence, and core-core electron correlations were studied using different strategies. This analysis has led to the final results in which the main balance electron correlation effects (mainly from VV substitutions) were included. This allows us to improve accuracy of the energy difference between different configurations considering the computational resources needed for the computations of such a complex system.

The rms deviations of the final results (using **SD 5d ZF^{MCDHF}** strategy) from the NIST or SE data for

states of the ground and excited configurations are 649 cm⁻¹, and 747 cm⁻¹, respectively.

Having analyzed convergence trends and dependencies of the gauge parameter G , we propose, for the Er²⁺ ion, to use transition rates in the Babushkin gauge.

There is a lack of atomic data for the lanthanides. The present study is a first step towards the goal to provide this data with an accuracy high enough for opacity modeling.

This research was funded by a grant (No. S-LJB-18-1) from the Research Council of Lithuania. Computations presented in this paper were performed at the High Performance Computing Center “HPC Sauletekis” of the Faculty of Physics at Vilnius University. DK is grateful to the support by NINS program of Promoting Research by Networking among Institutions (Grant Number 01411702).

REFERENCES

- Biémont, E., Garnir, H. P., Bastin, T., et al. 2001, Mon. Not. R. Astron. Soc., 321, 481
- Cowan, R. 1981, The Theory of Atomic Structure and Spectra (University of California Press, Berkeley, CA)
- Cowley, C. R., & Crosswhite, H. M. 1978, PASP, 90, 108
- Cowley, C. R., & Greenberg, M. 1987, PASP, 99, 1201
- Cowley, C. R., & Mathys, G. 1998, A&A, 339, 165
- Dyall, K., Grant, I., Johnson, C., Parpia, F., & Plummer, E. 1989, Computer Physics Communications, 55, 425
- Ekman, J., Godefroid, M., & Hartman, H. 2014, Atoms, 2, 215224. <http://dx.doi.org/10.3390/atoms2020215>

- Fischer, C. F., Gaigalas, G., Jansson, P., & Biero, J. 2019, *Computer Physics Communications*, 237, 184 .
<http://www.sciencedirect.com/science/article/pii/S0010465518303928>
- Fischer, C. F., Godefroid, M., Brage, T., Jönsson, P., & Gaigalas, G. 2016, *Journal of Physics B: Atomic, Molecular and Optical Physics*, 49, 182004
- Fritzsche, S., & Grant, I. 1994, *Physics Letters A*, 186, 152
- Gaigalas, G. 2020, *Computer Physics Communications*, 247, 106960. <http://www.sciencedirect.com/science/article/pii/S0010465519303157>
- Gaigalas, G., Fischer, C., Rynkun, P., & Jönsson, P. 2017, *Atoms*, 5, 6
- Gaigalas, G., Kato, D., Rynkun, P., Radžiūtė, L., & Tanaka, M. 2019, *The Astrophysical Journal Supplement Series*, 240, 29.
<https://doi.org/10.3847/2F1538-4365%2Faaf9b8>
- Gaigalas, G., & Rudzikas, Z. 1996, *Journal of Physics B: Atomic, Molecular and Optical Physics*, 29, 3303
- Gaigalas, G., Rudzikas, Z., & Fischer, C. F. 1997, *Journal of Physics B: Atomic, Molecular and Optical Physics*, 30, 3747
- Gaigalas, G., Rudzikas, Z., & Froese Fischer, C. 1998, *Atomic Data and Nuclear Data Tables*, 70, 139
- Gaigalas, G., Rudzikas, Z., Gaidamauskas, E., Rynkun, P., & Alkauskas, A. 2010, *Phys. Rev. A*, 82, 014502. <https://link.aps.org/doi/10.1103/PhysRevA.82.014502>
- Grant, I. P. 1974, *Journal of Physics B: Atomic and Molecular Physics*, 7, 1458
- . 2007, *Relativistic Quantum Theory of Atoms and Molecules* (Springer, New York)
- Jaschek, C., & Jaschek, M. 1995, *The Behavior of Chemical Elements in Stars* (Cambridge Univ. Press, Cambridge)
- Kasen, D., Metzger, B., Barnes, J., Quataert, E., & Ramirez-Ruiz, E. 2017, *Nature*, 551, 80
- Kato, D., Tong, X.-M., Watanabe, H., et al. 2001, *Journal of the Chinese Chemical Society*, 48, 525.
<https://onlinelibrary.wiley.com/doi/abs/10.1002/jccs.200100079>
- Kramida, A., Ralchenko, Y., Reader, J., & NIST ASD Team. 2019, *NIST Atomic Spectra Database* (ver. 5.7.1), [Online]. Available: <https://physics.nist.gov/asd> [2020, January 17]. National Institute of Standards and Technology, Gaithersburg, MD., ,
- Lindgren, I., & Morrison, J. 1982, *Atomic Many-Body Theory* (Springer-Verlag Berlin Heidelberg, New York)
- Martin, W. C., & Zalubas, R. and Hagan, L. 1978, *Atomic Energy Levels - The Rare-Earth Elements* (Nat. Bur. Stand., U.S.)
- McKenzie, B., Grant, I., & Norrington, P. 1980, *Computer Physics Communications*, 21, 233
- Olsen, J., Godefroid, M. R., Jönsson, P., Malmqvist, P. A., & Fischer, C. F. 1995, *Phys. Rev. E*, 52, 4499
- Papouliou, A., Ekman, J., Gaigalas, G., et al. 2019, *Atoms*, 7, 106. <http://dx.doi.org/10.3390/atoms7040106>
- Rudzikas, Z. 2007, *Theoretical Atomic Spectroscopy* (Cambridge University Press, Cambridge, UK)
- Spector, N. 1973, *Journal of the Optical Society of America*, 63, 358
- Tanaka, M., Kato, D., Gaigalas, G., & Kawaguchi, K. 2019, *ApJ*, submitted
- Tanaka, M., Kato, D., Gaigalas, G., et al. 2018, *ApJ*, 852, 109
- Wyart, J.-F., & Bauche-Arnoult, C. 1981, *Physica Scripta*, 22, 583
- Wyart, J.-F., Blaise, J., & P., C. 1974a, *Physica Scripta*, 9, 325
- Wyart, J.-F., Blake, J., Bidelman, W. P., & Cowley, C. R. 1997, *Physica Scripta*, 56, 446
- Wyart, J.-F., Koot, J. J. A., & Van Kleef, T. A. M. 1974b, *Physica C*, 77, 159
- Ynnerman, A., & Fischer, C. F. 1995, *Phys. Rev. A*, 51, 2020.
<https://link.aps.org/doi/10.1103/PhysRevA.51.2020>
- Zhang, W., Palmeri, P., Quinet, P., & Biémont, E. 2013, *A&A*, 551, A136.
<https://doi.org/10.1051/0004-6361/201220918>